Silencing of Hepatic AATF Ameliorates Metabolic Dysfunction Associated Steatohepatitis by Promoting Fatty Acid β-Oxidation in Experimental models

Akshatha N. Srinivas[1], Diwakar Suresh[1], Manju Moorthy[2], Gopalkrishna Ramaswamy[2], Prasanna Kumar Santhekadur[1], Deepak Suvarna[3], and Divya P. Kumar[1]*

[1]Department of Biochemistry, CEMR, JSS Medical College, JSS Academy of Higher Education and Research, Mysuru, Karnataka, India

[2]TheraCUES Innovations Pvt. Ltd, Bangalore, India

[3]Department of Gastroenterology, JSS Medical College and Hospital, JSS Academy of Higher Education and Research, Mysuru- 570015, Karnataka, India

*Correspondence:
Dr. Divya P. Kumar
Associate Professor
Department of Biochemistry
JSS Medical College, JSS AHER
SS Nagar, Mysuru- 570015
Karnataka, India
Email: divyapk243@gmail.com/
divyapkumar@jssuni.edu.in

ABSTRACT

Background: Metabolic dysfunction-associated steatotic liver disease (MASLD) affects 30% of the global population and has emerged as a significant public health concern. It is a multifactorial pathological condition driven by various molecular drivers. Thus, identifying and understanding the molecular drivers involved in MASLD pathogenesis is essential for developing targeted therapeutic strategies.
Aim: To elucidate the role of apoptosis antagonizing transcription factor (AATF) as a molecular driver in the pathogenesis of MASLD and its underlying mechanisms.
Methods: A preclinical murine model resembling human MASLD was employed, in which C57Bl/6 mice were fed either a chow diet with normal water (CD) or a western diet with sugar water (WD). After 12 weeks, mice were injected via the tail vein with AAV8 serotype particles and randomized into four groups: (i) CD with AAV8-TBG-Null, (ii) CD with AAV8-TBG-siAATF, (iii) WD with AAV8-TBG-Null (WD control), and (iv) WD with AAV8-TBG-siAATF (WD siAATF). Biochemical, histological, and molecular analyses were performed using serum and liver tissues. Untargeted metabolomics was carried out in the liver tissues of the experimental MASLD.
Results: AATF was upregulated in cellular and preclinical models of MASLD. Liver-specific silencing of AATF reduced body weight, liver weight, and insulin resistance in WD mice compared to WD controls but had no effect on CD mice. Biochemical, histological, and molecular analyses showed reduced liver injury, steatosis, inflammation, and fibrosis in AATF-silenced WD mice. Furthermore, untargeted metabolomics revealed increased levels of glycerophospholipids, such as phosphatidylcholines, phosphatidylserines, and phosphatidylethanolamines, in the WD siAATF mice. Consistently, expression of hepatic carnitine palmitoyl transferase (CPT1) and peroxisome proliferator-activated receptor alpha/gamma (PPAR α/γ), which promote fatty acid beta oxidation, was upregulated in the WD siAATF compared to WD controls.
Conclusion: These findings show a molecular link between AATF and hepatic lipid metabolism, implying that AATF could be a promising therapeutic target for MASLD.

KEYWORDS

Apoptosis antagonizing transcription factor, metabolic dysfunction-associated steatotic liver disease, adeno-associated virus 8, fatty acid β-oxidation, metabolomics

ABBREVIATIONS

MASLD, metabolic dysfunction-associated steatotic liver disease; NAFLD, nonalcoholic fatty liver disease; MASH, metabolic dysfunction-associated steatohepatitis; NASH, nonalcoholic steatohepatitis; HCC, hepatocellular carcinoma; CVD, cardiovascular disease; CKD, chronic kidney disease; AATF, apoptosis antagonizing transcription factor; DIAMOND, diet-induced animal model of NAFLD; STAT3, signal transducer and activator of transcription 3; MCP-1, Monocyte chemoattractant protein-1; KLF4, Krupple-like factor 4; SP1, Specificity protein 1; PPAR α/γ, peroxisome proliferator-activated receptor alpha/ gamma; CPT-1/2, carnitine palmitoyltransferase 1/2; AMPK, adenosine monophosphate-activated protein kinase; mTOR, mammalian target of rapamycin; NAS Score: NAFLD activity score; GTT, glucose tolerance test; HOMA-IR, homeostatic model assessment of insulin resistance; ITT, insulin tolerance test; AST, aspartate transaminase; ALT, alanine transaminase; TC, total cholesterol; TG, total triglycerides; LDL, low-density lipoprotein; ECL, enhanced chemiluminescence; HRP, horseradish peroxidase; FFPE, formalin-fixed, paraffin-embedded; FBS Fetal bovine serum; LC-MS, liquid chromatography-mass spectrometry; UHPLC, ultrahigh performance liquid chromatography; MeOH, methanol; SIRT1, silent information regulator 1; TIMP3, tissue inhibitor of metalloproteinase 3; TACE, TNF-alpha converting enzyme; MASL, metabolic dysfunction-associated steatotic liver; TBG, thyroxine-binding globulin; AAV8, adeno-associated virus 8; CDNW, chow diet normal water; WDSW, western diet sugar water; PA, Sodium Palmitate; SO, Sodium Oleate; TGF β, transforming growth factor β; Grp78; 78 kDa glucose-regulated protein; CHOP, C/EBP homologous protein; Atf4, activating transcription factor 4; TNF-α, tumor necrosis factor-alpha; IL-6, interleukin-6; IL-1β, interleukin-1β; JNK, c-Jun N-terminal kinases; ERK1/2, extracellular signal-regulated kinase 1/2; PGC-1α, peroxisome proliferator-activated receptor-gamma coactivator; MCAD, medium-chain acyl-coenzyme A dehydrogenase; LysoPC, lysophosphatidylcholines; PCA, principal component analysis; VIP, variable importance in the projection.

INTRODUCTION

Metabolic dysfunction-associated steatotic liver disease (MASLD), formerly termed non-alcoholic fatty liver disease (NAFLD), stands as the prevailing chronic liver ailment impacting more than 30% of the adult population worldwide (1,2). It notably afflicts individuals with obesity and type 2 diabetes, emerging as a primary contributor to advanced liver disease and hepatocellular carcinoma (HCC) (3,4). MASLD encompasses a spectrum of advancing steatotic liver conditions, spanning from benign metabolic dysfunction-associated steatotic liver (MAFL) to steatohepatitis (MASH), presenting with varying degrees of liver fibrosis that could advance to cirrhosis (5). MASLD not only heightens the likelihood of liver-related complications such as cirrhosis, end-stage liver disease, and hepatocellular carcinoma (HCC) but also escalates the risk of multiple extraneous manifestations, including cardiovascular disease (CVD), chronic kidney disease (CKD), and specific forms of extrahepatic cancers (6). As MASLD progresses to the end stage of liver disease, treatment options become increasingly limited, often leading to consideration for liver transplantation (7). Early detection, and intervention, are therefore paramount. While lifestyle modifications remain fundamental to managing the condition, pharmacological treatments can complement these interventions (8). Despite numerous clinical studies, the pathogenesis of MASLD remains elusive, and the mechanisms underlying its occurrence and progression are not yet fully understood (9). Therefore, elucidating the molecular pathways involved in MASLD pathogenesis is crucial for identifying potential therapeutic targets.

MASLD manifests with the accumulation of lipids in the liver, stemming from disturbances in both lipid uptake (from circulating sources or de novo synthesis) and lipid disposal (via fatty acid oxidation or secretion of triglyceride-rich lipoproteins) (10). This disruption results in the buildup of lipotoxic compounds, cellular stress, injury, and fibrosis (10,11). The regulation of lipid metabolism is complex and multifaceted, involving various factors like membrane transporters, metabolic enzymes, and transcriptional regulators (12). Glycerophospholipids, a subclass of phospholipids that are the major constituents of cell membranes, play a key role in lipid metabolism, and alterations in the composition of glycerophospholipids have been reported in individuals with MASLD (13,14). Phosphatidylcholine (PC), phosphatidylethanolamine (PE), phosphatidylserine (PS), phosphatidylinositol (PI), and cardiolipin (CL) are a diverse array of glycerophospholipids that are well studied for their role in cell signaling and lipid metabolism (14). Glycerophospholipids are involved in inflammatory, oxidative stress, and bile acid metabolism pathways, which are key drivers in the disease pathogenesis of MASLD. Furthermore, glycerophospholipids, in addition to contributing to the integrity of the mitochondrial membrane, also play a role in the beta-oxidation of fatty acids (15). It is observed that, in MASLD patients, reduced fatty acid β-oxidation in the liver results in insufficient counteraction to the lipotoxic effects induced by harmful lipids (15). Studies have shown that peroxisome proliferator-activated receptors alpha/gamma (PPAR-α/γ) and carnitine palmitoyltransferase-1 alpha (CPT-1α), major regulators of fatty acid β-oxidation, are downregulated in MASLD (16). Interestingly, activation of PPARγ-mediated autophagy via the AMPK/mTOR pathway led to decreased steatosis, increased rates of fatty acid β-oxidation, and ultimately downregulated hepatic lipid degeneration in obese mice (17). Recent studies have demonstrated the efficacy of CPT1α gene therapy aimed at enhancing fatty acid β-oxidation in the liver, resulting

in a reduction of steatosis in mice (18). Collectively, these studies suggest that patients with MASLD exhibit decreased fatty acid β-oxidation, and rejuvenating this process could represent a promising avenue for MASLD treatment.

Apoptosis antagonizing transcription factor (AATF) is a multifaceted transcription factor recognized for its pivotal involvement in essential cellular functions (19). It serves as a dynamic regulator of fundamental cellular processes such as transcriptional control, cell cycle and apoptosis regulation, ribosome biogenesis, and response to cellular stress (19) AATF protects cells from oxidative stress, ER stress, DNA damage, and hypoxia by modulating the cell cycle, autophagy, and apoptosis (20). The widely studied role of AATF is apoptosis regulation exerted by activation of antiapoptotic and inhibition of proapoptotic pathways (21). Pathologically, AATF has been implicated in numerous cancer types, including leukemia, breast cancer, neuroblastoma, lung cancer, and colon cancer (22-24). Our previous investigations have revealed elevated levels of hepatic AATF in HCC, where it plays a significant role in promoting tumor angiogenesis (25). Studies have also demonstrated the inhibitory effects of curcumin on MASH-HCC by downregulating AATF via the KLF4-SP1 pathway (26). We recently explored the involvement of the SIRT1-TIMP3-TACE axis in AATF upregulation, with subsequent TACE inhibition leading to AATF downregulation and attenuation of MASH-associated liver tumorigenesis (27). However, the mechanistic role of AATF in the pathophysiology of MASH remains poorly understood.

In this study, we examined the novel role of AATF in diet-induced experimental MASH. We found that AATF expression positively correlated with the MASLD spectrum, and liver-specific knockdown of AATF significantly improved MASH by reducing steatosis, inflammation, and fibrosis. Additionally, we investigated the effect of hepatic silencing of AATF on MASH through untargeted metabolomics. In the current study, we integrated biochemical and molecular parameters and metabolomics to provide novel insights into the role of AATF in hepatic metabolism. These findings collectively shed light on the unexplored mechanistic role of AATF in regulating lipid metabolism.

MATERIALS AND METHODS

Materials

Customized chow diet and western diet were purchased from Research Diets Inc. (USA). Biochemical assay kits were from Monlab tests (Spain). Sodium Palmitate, Sodium Oleate, Oil Red O solution, Liberase, antibody to AATF, TRIzol reagent, RIPA buffer, and Picrosirius red stain were from Sigma-Aldrich (USA). FBS, glutamine, collagen, penicillin-streptomycin solution, verso cDNA synthesis kit, and DyNamo Colorflash SYBR green kit from Thermo Fisher Scientific (USA). Primers were from Integrated DNA Technologies (IDT). Western blotting materials from Bio-Rad and western bright ECL HRP substrate. Cell culture media, supplements, glucose, fructose, cell strainer, and hematoxylin were from HiMedia Laboratories. Antibodies to pJNK, JNK, pErk1/2, and Erk1/2 were from Santa Cruz Biotechnology; antibodies to F4/80, Desmin, and β-actin were from Cell Signaling Technologies.

Animal study

Male C57Bl/6NCrl mice aged 6 weeks procured from Hylasco Biotechnology Pvt. Ltd. (Charles River Laboratories, Hyderabad, Telangana, India) were used for the study. All the mice were accommodated in the central animal housing facility at the Center for Experimental Pharmacology and Toxicology, JSS AHER following a 12-hour light-dark cycle, consistent with previously established protocols (28). Following one week of acclimatization, study protocols were commenced. All animal-related procedures adhered to the guidelines sanctioned by the Committee for the Purpose of Control and Supervision of Experiments on Animals (CPCSEA), Govt. of India (JSSAHER/CPT/IAEC/118/2022).

Diet-induced MASLD model:

After a week of acclimatization, the mice were fed with either a chow diet or a western diet with high fat, high sucrose, and high cholesterol (WD, 21% fat, 41% sucrose, and 1.25% cholesterol by weight, Research Diet, Inc. USA) along with normal water or high sugar (18.9 g/L d-glucose and 23.1 g/L d-fructose) containing drinking water ad libitum for 24 weeks. Mice were continuously monitored for food intake, water intake, and body weight. After 24 weeks, mice were euthanized, and blood and tissues were collected for further analysis.

***In vitro* model of steatosis**

Huma hepatic cells HepG2 and Huh7 cells were a kind donation from Dr. Suresh Giri, Zydus Cadila, Gujrath, India. HepG2 cells were cultured in DMEM containing 1 g/L glucose, and Huh7 cells were cultured in DMEM containing 4.5 g/L glucose. The culture media were supplemented with 10% fetal bovine serum, L-glutamine, and 100 U penicillin-streptomycin and incubated at 37 ^{0}C in 5% CO_2.

To develop an *in vitro* model of steatosis, cells were cultured up to 50% confluency in culture plates, followed by treatment with free fatty acids: 0.5 mM sodium oleate (SO), 0.5 mM sodium palmitate (SP), or a mixture of both SO and SP (SP+SO) in a 1:1 ratio in 5% fatty acid-free BSA containing culture media. After 24 hours of treatment, the cells were assessed for lipid droplets using Oil Red O staining. For all the experiments, cells were treated with free fatty acids for 24 hours, and the cell pellets were collected for RNA isolation or protein lysate preparation.

AAV expression system

Liver gene expression was modulated using AAV-mediated gene transfer technology as defined previously (29). The siRNA sequences targeting AATF were incorporated into an adeno-associated virus (AAV) vector, under the regulation of liver-specific thyroxine-binding globulin (TBG) promoter. AAV8-TBG-siAATF and AAV8-TBG-null constructs were generated by packaging into serotype 8, titrated by Applied Biological Materials Inc. (ABM).

Hepatocyte-specific silencing of AATF in experimental MASH

The mice were fed either a chow diet normal water (CD) or a western diet sugar water (WD). After 12 weeks of dietary intervention, mice were injected via the tail vein with 1×10^{11} Genome copies of AAV8 serotype particles and randomized into four groups: (i) CDNW with AAV8-TBG-Null, (ii) CDNW with AAV8-TBG-siAATF, (iii) WDSW with AAV8-TBG-Null, and (iv) WDSW with AAV8-TBG-siAATF. The

same dietary regimen was followed until the end of 24 weeks. Throughout the study, mice were continuously monitored for food intake, water intake, and body weight. Glucose tolerance test (GTT) and insulin tolerance test (ITT) were performed during the study period. After 24 weeks, mice were euthanized under fasting conditions, followed by blood and tissue collection for further analysis.

Isolation of primary mouse hepatocytes

Primary hepatocytes were isolated from the livers of mice injected with AAV8-TBG-Null and AAV8-TBG-siAATF following previously established protocols (29). Briefly, mice were anesthetized, and the inferior vena cava was cannulated. Liver perfusion was carried out using pre-warmed perfusion buffer followed by the digestion buffer containing 25 µg/ml Liberase. The isolated hepatocytes were then filtered through a 70-micron cell strainer and purified via centrifugation in DMEM at 50g for 5 minutes at room temperature. Percoll gradient separation was employed to isolate hepatocytes from nonparenchymal cells. The isolated cells were suspended in DMEM supplemented with 10% FBS and 100U penicillin-streptomycin. Collagen-coated plates were utilized for cell culture in William's E medium.

Glucose and Insulin tolerance tests

Mice were fasted overnight, or 5-6 hours for GTT (glucose tolerance test) and ITT (insulin tolerance test), respectively. The basal level of blood glucose was measured using a glucometer. Further, mice were subjected to oral administration of glucose (1 g/kg body weight) and intraperitoneal injection of insulin (0.75 U/kg body weight). Venous tail blood samples were taken at different intervals between 0 and 120 minutes to measure the blood glucose level.

Biochemical analysis

Blood collected from the fasting mice was centrifuged at 1500 g for 15 min at 4°C. The serum levels of aspartate transaminase (AST), alanine transaminase (ALT), total cholesterol (TC), total triglycerides (TG), and LDL-cholesterol were measured using commercial kits according to the manufacturer's protocol.

Histological analysis

Liver tissues were subjected to formalin fixation and paraffin blocks were prepared. 4µm tissue sections were used for hematoxylin and eosin staining to assess the liver morphology. For pathological grading, stained liver sections were scored by pathologists according to the MASLD activity score comprising the sum of steatosis (0-3), lobular inflammation (0-3), and hepatocyte ballooning (0-2). A cumulative activity score of ≥5 was indicative of MASH.

Oil Red O staining

Oil Red O staining was performed using frozen liver tissues. Cryosections, 12-µm thick, were fixed with 10% formaldehyde for 5 minutes and washed with distilled water. Further, the slides were incubated with 60% isopropanol and Oil Red O solution for one hour. After rinsing off excess stain with distilled water, nuclei were counterstained with hematoxylin. The slides were then mounted, and images were captured using the Leica microscope. For quantitative analysis, the areas of lipid droplets were quantified using ImageJ software.

Picrosirius red staining

The FFPE liver tissue sections were subjected to deparaffinization and rehydration using xylene, followed by decreasing percentages of ethanol. The slides were first stained with hematoxylin for 2 minutes, followed by incubation with the picrosirius red solution for 1 hour. Slides were washed in 0.5% acidified water and mounted. The images were captured using the Leica microscope and quantified using ImageJ software.

Immunohistochemistry

Immunohistochemistry was carried out according to the standard protocol. Briefly, after deparaffinization and rehydration, FFPE liver tissues were subjected to antigen retrieval with citrate buffer (pH 6) at 94°C for 15 minutes. Following this, the tissue sections were blocked with 3% hydrogen peroxide and normal goat serum for 2 hours. Primary antibodies (AATF at 1:500, F4/80 at 1:100, and Desmin at 1:500 dilutions) were used to stain the respective tissue sections overnight at 4°C in a humidified chamber. The detection of signals was accomplished using the Polyexcel HRP/DAB detection system (PathnSitu, Biotechnologies). Images were captured using the Leica microscope, and quantitative analysis was conducted using ImageJ software.

ELISA

Serum insulin and TNFα levels were quantified using mouse ELISA kits according to the manufacturer's instructions.

Immunoblot analysis

Liver tissues and cell pellets were dissolved in RIPA buffer containing protease/phosphatase inhibitor cocktail. The lysates were obtained by centrifugation at 12000 rpm at 4^0C for 20 minutes. Protein concentration was estimated by Bradford's protein estimation method. Equivalent amounts of protein were resolved in SDS-PAGE, followed by transfer into the nitrocellulose membrane. Blots were blocked in 5% nonfat dry milk for 1 hour and probed with primary antibodies of interest (anti-AATF 1:1000, anti-β-actin 1:1000, anti-pJNK, anti-JNK, anti-pERK1/2, and anti-ERK1/2 1:100) overnight at 4^0C and secondary antibodies for 2 hours at room temperature. Blots were visualized using Western Bright ECL HRP substrate in the UVitec Alliance Q9 chemiluminescence imaging system and analyzed for densitometric measurements in ImageJ software. The band intensity was normalized with the respective endogenous control.

Quantitative real-time PCR

Total RNA was extracted from the frozen live tissues or cell pellets using TriZol reagent according to the manufacturer's instructions. RNA was quantified using the nanodrop spectrophotometer and reverse transcribed using the verso cDNA synthesis kit following the manufacturer's protocol. Relative gene expressions were assessed using quantitative real-time PCR using the Rotor-Gene Q 5plex HRM system. DyNamo Colorflash SYBR green kit with 0.5 mM primers (IDT), and 50 ng of cDNA in a 20 µl reaction volume were used to set up the reaction. The mRNA levels of selected genes were calculated after normalization to β-actin by using the $2^{(-\Delta\Delta C(T))}$ method. Primer sequences are provided in Supplementary Table 1.

Untargeted metabolomics

i. Metabolite extraction and LC-MS analysis:

Metabolites were extracted following previously established protocols (30). Briefly, liver tissues were lyophilized in a vacuum freeze dryer for 24 hours, and 50 mg of samples were homogenized with 50 mM ammonium bicarbonate (3:1 w/v). Samples were extracted in cold methanol by centrifugation at 18,000× g for 15 minutes at 4°C. Supernatants are dried and reconstituted in MeOH: water (3:1 v/v) for LC/MS analysis. The hepatic metabolome was analyzed using a Vanquish UHPLC system (Thermo Fisher) coupled with an Orbitrap Eclipse Tribrid mass spectrometer (Thermo Fisher). Samples were separated on an RP column, 2.1 x 150 mm, 1.8 um particle size, and 0.3 mL/min flow rate with two eluents for positive and negative polarity modes.

ii. Metabolomics data analysis

The data processing was done using the Compound Discoverer 3.3 software (Thermo Fisher Scientific). A pre-existing workflow template titled 'Untargeted Metabolomics with Statistics Detect Unknowns with ID using Online Databases and mzLogic' was used to identify the differences between samples. For identification, the mass tolerance was 5 ppm, and the retention time tolerance was 0.2 min. The minimum peak intensity was 10,000, and the chromatographic S/N threshold was 1.5. The solvent blanks were used to create exclusion lists, mark background components, and filter the background components from the results table. A pooled quality control (QC) sample was used for compound identification only.

To visualize the similarity between the metabolomic profiles of the samples from different groups, principal component analysis (PCA) and heatmap plots were generated. All the analyses were conducted based on the compound's peak areas. Differential metabolite analysis was conducted using a Student's t test, considering p value<0.05 as significant and log2 foldchange >= |1| as either an upregulated or downregulated metabolite. The log2 foldchange per metabolite was calculated as ratio between group areas, transformed to log2 scale, with group area being calculated as the median of compound area per sample within the group. The up- or down-regulated metabolites were visualized using volcano plots. P-values were adjusted for multiple testing using the Benjamini Hochberg correction for false discovery rate.

We applied the GSEA algorithm against the Kyoto Encyclopedia of Genes and Genomes (KEGG) Mus musculus (House Mouse) pathway library, lipid superclass and subclass. Significant pathways (p<0.05) from the GSEA method were analyzed further. Pathway enrichment against the small molecule pathway database (SMPDB) database was performed separately for upregulated and downregulated metabolites using MetaboAnalyst 6.0. For overlaying the regulation of metabolites involved in the glycerophospholipid metabolism pathway, the compound list and pathway were accessed from the KEGG database and visualized using the Pathview R package. In order to visualize the metabolic network, we used MetScape (http://metscape.ncibi.org./), the Cytoscape plugin to identify the interaction between the metabolites involved in the glycerophospholipid metabolism pathway.

Statistical Analysis

Statistical analyses were performed using GraphPad Prism 6.0 software (GraphPad, Inc., La Jolla, CA, USA). Data were represented as the mean ± standard error of the mean. Statistical significance was analyzed using Student's t-test for two groups or analysis of variance (ANOVA) with post hoc Bonferroni correction for multiple comparisons and p values < 0.05 (*/#) or < 0.001 (**/##) were considered significant.

RESULTS

AATF is highly expressed in experimental models of metabolic dysfunction-associated steatotic liver disease

We initially determined the hepatic AATF expression in the cellular model and also across different stages of MASLD in an *in vivo* murine model. Free fatty acids, such as sodium palmitate (PA) or sodium oleate (SO), were used to mimic liver steatosis in the human hepatic cell lines HepG2 and Huh7. Upon confirmation of lipid accumulation as visualized by Oil Red O staining (**Figure 1A**), AATF expression was determined. Our observations revealed a significant upregulation of AATF both at mRNA and protein levels in the *in vitro* model. Furthermore, we employed a preclinical model of MASLD, which developed MAFL at 12 weeks and MASH at 24 weeks in western diet sugar water mice compared to chow diet normal water mice (**Figure 1E**). AATF mRNA and protein levels were notably elevated at MAFL and MASH stages compared to the control (**Figure 1F and 1G**). These collective findings underscore the upregulation of AATF during the progressive stages of MASLD, implicating its potential significance in disease progression.

Silencing of hepatic AATF prevents WDSW-induced steatosis, steatohepatitis, and fibrosis

To assess the effect of AATF on liver metabolism, we silenced AATF expression in the hepatocytes of mice using liver-directed AAV8 under the control of the thyroxine-binding globulin (TBG)-mediated gene silencing system. Mice were fed chow diet normal water (CD) or western diet sugar water (WD). After 12 weeks, all mice received tail vein injections of either AAV8-TBG-Null or AAV8-TBG-siAATF and were monitored for an additional 12 weeks (**Figure 2A**). The expression of AATF was validated in various tissues of mice, such as the liver, adipose tissue, heart, kidney, pancreas, and spleen. We found reduced AATF expression only in the liver tissue of AAV8-TBG-siAATF mice compared to AAV8-TBG-Null mice (**Figure 2B and 2C**). Additionally, we confirmed AATF silencing specifically in hepatocytes, with no effect on non-parenchymal cells (**Figure 2D**).

Hepatic AATF silencing for 12 weeks significantly reduced body weight, liver weight, liver-body ratio, and body fat mass compared to those treated with AAV8-TBG-Null in WD mice but had no effect in CD mice (**Figure 2E- 2H**). AATF silencing also improved glucose tolerance and insulin sensitivity, as demonstrated by the glucose tolerance test (GTT) and the insulin tolerance test (ITT), respectively, in WD mice (**Figure 2I and 2J**). Notably, WD siAATF mice exhibited decreased blood glucose levels, fasting insulin levels, and homeostatic model assessment for insulin resistance (HOMA-IR) compared to WD control mice, indicating alleviation of high-fat and high sugar diet-induced glucose metabolism exacerbation and insulin

resistance (**Figure 3A- 3C**). Furthermore, hepatic AATF silencing led to notable reductions in serum levels of ALT, AST, total cholesterol, triglycerides, and LDL-cholesterol in WD mice compared to WD controls (**Figure 3D- 3H**). No significant differences were observed in CD mice treated with AAV8-TBG-siAATF compared to AAV8-TBG-Null mice. Macroscopic examination revealed healthier liver morphology in WD siAATF mice compared to WD controls (**Figure 3I**). Histological analysis of liver sections showed decreased steatosis and substantial improvement in steatohepatitis (MASH) upon AATF silencing compared to controls in WD mice (**Figure 3J**). Similar results were obtained with Oil Red O staining of liver sections, where there was reduced intracellular lipid droplet accumulation in WD siAATF mice compared to WD controls (**Figure 3K**), indicating that hepatic AATF inhibition improves metabolic health by ameliorating liver injury and dysregulated lipid metabolism.

Consistent with these findings, histological scoring for steatosis, lobular inflammation, and hepatocyte ballooning was reduced in hepatic AATF-silenced WD mice, with an improvement in MASLD activity score compared to WD controls (**Figure 4A- 4D**). More interestingly, we observed reduced fibrosis in WD siAATF mice compared to WD controls, as evidenced by picrosirius red staining (**Figure 4E**). In addition, hepatic stellate cell activation marked by desmin and α-SMA overexpression was attenuated in WD siAATF mice (**Figure 4F and 4G**). The key markers for liver fibrosis, including Col1A1, Col3A1, and TGF-β, were downregulated in WD siAATF mice, suggesting that AATF silencing reduces fibrogenic activation in WD mice (**Figure 4H- 4J**).

AATF silencing alleviates hepatic ER stress and inflammation in Experimental MASH

Endoplasmic reticulum (ER) stress plays a prime role in the pathogenesis of MASH by promoting hepatic inflammation and fibrosis. Several factors contribute to ER stress, including lipid accumulation in hepatocytes, mitochondrial dysfunction, and oxidative stress (31). In our investigation, we explored the impact of hepatic AATF silencing on the expression of key ER stress markers. Remarkably, in WD siAATF mice, we found significant downregulation in the mRNA levels of CHOP, Grp78, PERK, and ATF4 compared to WD controls (**Figure 5A- 5D).**

Furthermore, elucidating the intricate crosstalk between ER stress and inflammation, our study revealed that ER stress activation triggers inflammatory signaling pathways, notably stress kinases, leading to the release of pro-inflammatory cytokines in WD control mice. This increase in inflammation was remarkably reduced by the silencing of hepatic AATF in WD mice, as evidenced by the reduced expression of pro-inflammatory cytokines IL-6, IL-1β, and TNF-α (**Figure 5E- 5H**). Concurrently, phosphorylation of JNK and Erk1/2 was noticeably diminished in WD siAATF mice compared to WD controls (**Figure 5I and 5J**). The immunostaining for the mouse macrophage marker F4/80 corroborated these findings, showing a marked reduction in response to AATF knockdown in WD mice (**Figure 5K**). These findings signify AATF as an important mediator for ER stress-induced hepatic inflammation.

Effect of hepatic AATF silencing on metabolic profiles in Experimental MASH

Hepatic metabolite profiling was conducted through an untargeted metabolomics analysis, where raw mass spectra peaks were meticulously annotated using mzCloud (ddMS2) and ChemSpider (formula or exact mass). PCA and PLS-DA techniques were utilized to discern differences between experimental groups and identify the variations that contribute to these classifications. Notably, there was significant separation of liver metabolites between the WD siAATF and WD control groups, as well as significant separation between the WD control and CD control groups, as depicted by both the Principal Component Analysis (PCA) and PLS-DA plots (**Figure 6A and 6B).** Further, unsupervised hierarchical clustering analysis of differentially expressed metabolites (DEMs) revealed a distinct pattern between WD siAATF and WD control (WDC) in contrast to CD siAATF and CD control (CDC) **(Figure 6C)**. Univariate analysis identified 487 metabolites altered in WD siAATF, of which 412 were upregulated in contrast to 197 upregulated metabolites in WD control. Similarly, 867 metabolites were downregulated in WD control mice, whereas only 75 metabolites were downregulated in WD siAATF mice, clearly showing marked differences in the metabolome profiling upon hepatic AATF silencing. Subsequently, data underwent normalization and filtering based on significant differential metabolite analysis between groups (FC >1 and <1, P<0.05 were considered significant). Consistently, the volcano plots also showed a similar distribution of differentially altered metabolites between WD control vs. CD control **(Figure 6E)** and WD siAATF vs. WD control **(Figure 6F).**

Identification of differentially expressed metabolites between WD siAATF and WD control samples

To comprehend the significance of the dysregulated metabolites in relation to specific biological processes, a metabolic pathway analysis was conducted using the online tool MetaboAnalyst 6.0. This analysis included all metabolites that were found to be significant ($p < 0.05$). The enrichment analysis between WD control and CD control (**Figure 7A**) revealed metabolic processes involved in the onset of MASH, including gluconeogenesis, bile acid synthesis, pyrimidine metabolism, and steroidogenesis. On the other hand, KEGG pathway analysis revealed that 74 pathways were enriched by the DEMs in the WD siAATF vs. WD control groups. Of these, glycerophospholipid metabolism, ether lipid metabolism, nicotinamide metabolism, linoleic acid metabolism, riboflavin metabolism, and pyruvate metabolism were significantly upregulated upon hepatic silencing of AATF. In contrast, branched-chain amino acid biosynthesis, sulfur metabolism, and glycerolipid metabolism were downregulated **(Figure 7B)** Further, DEMs were enriched against lipid superclass within the KEGG database, which unveiled the upregulation of glycerophospholipids (glycerophosphocholines, glycerophosphoserines, and glycerophosphoethanolamines), fatty esters, and eicosanoids in WD siAATF mice **(Figure 7C).** Delving deeper into lipid subclass analysis, phosphatidylcholine (PC), phosphatidylserine (PS), phosphatidyl ethanolamine (PE), lysoPC, lysoPE, lysoPS, and vitamin D3 were elevated in WD siAATF mice **(Figure 7D).** Of particular interest, DEMs involved in glycerophospholipid metabolism were represented as a heatmap **(Figure 7E).**

A network analysis of putative interacting proteins of the metabolites significantly altered by hepatic silencing of AATF in WD mice was identified and enriched in the glycerophospholipid metabolism pathway in the KEGG database **(Figure 8A)**. Of particular importance, levels of phosphocholine, phosphatidylcholine (PC), lysophophatidylethanolamine (LPE), and lysophosphatidylcholine (LPC) were all significantly increased in WD siAATF mice compared to WD controls (**Figure 8C)**. To gain deeper insights into the biological functions of the differentiated metabolites, a functional relationship network was constructed utilizing Metscape. The resulting network revealed that most of the metabolites were primarily involved in the metabolism of glycerophospholipids, linoleate, and phosphatidyl inositol **(Figure 8C).** Collectively, these findings underscore the profound impact of AATF silencing on liver metabolites, particularly in the upregulation of glycerophospholipid biosynthesis, notably in PC and PE species.

Beta-oxidation of fatty acids is intricately linked to the pathogenesis of MASH. Dysregulation of beta-oxidation pathways contributes to hepatic lipid accumulation, oxidative stress, and inflammation, driving the progression of the disease (32). Along similar lines, our studies revealed the upregulation of metabolites involved in mitochondrial beta-oxidation pathway alongside the biosynthesis of phosphatidylcholine (PC) in WD siAATF through pathway enrichment analysis using the SMPB database (**Figure 9A**). Consistently, metabolites involved in MASH development pathways were downregulated in WD siAATF mice (**Figure 9B)**. Thus, we hypothesized that AATF silencing promotes beta-oxidation of fatty acids, thereby ameliorating MASH. In accordance with our hypothesis, our findings revealed notable upregulation of key genes associated with the beta-oxidation pathway, including carnitine palmitoyltransferase-1 alpha (CPT1α), a pivotal enzyme facilitating fatty acid transport into mitochondria, and the regulators of beta-oxidation, peroxisome proliferator-activated receptors alpha and gamma (PPAR-α and PPAR-γ), in WD siAATF mice compared to controls. Additionally, the expression levels of peroxisome proliferator-activated receptor gamma coactivator 1-alpha (PGC1α), a coactivator of PPAR-α and PPAR-γ, were found to be elevated in WD siAATF mice, indicative of enhanced mitochondrial fatty acid uptake and oxidation (**Figure 9C**). Collectively, hepatic silencing of AATF ameliorates MASH by promoting β-oxidation of fatty acids (**Figure 9D**).

DISCUSSION

Metabolic dysfunction-associated steatotic liver disease (MASLD), commonly known as non-alcoholic fatty liver disease (NAFLD), is a multifactorial condition influenced by various molecular drivers (5). Dysregulation of lipid metabolism is a hallmark of MASLD. Increased influx of free fatty acids (FFAs) from adipose tissue and dietary sources, along with impaired fatty acid oxidation and export of triglycerides from the liver, contribute to hepatic steatosis (10). Insulin resistance in hepatocytes leads to impaired suppression of gluconeogenesis and increased lipogenesis, promoting hepatic lipid accumulation (33). Several factors associated with metabolic dysfunction, including lipid accumulation, oxidative stress, and insulin resistance, can trigger ER stress in hepatocytes (31). Inflammatory pathways play a crucial role in the progression of MASLD from simple steatosis to MASH. Activation of inflammatory signaling pathways leads to the production of pro-inflammatory cytokines and chemokines, contributing to hepatocyte injury and fibrosis (34). Thus, identifying and

understanding the molecular drivers involved in MASLD pathogenesis is essential for developing targeted therapeutic strategies aimed at preventing disease progression and improving clinical outcomes for patients with MASLD. The evolving understanding of the disease underscores the urgent need for new therapeutic targets. The complex pathophysiology of MASLD involves multiple metabolic, inflammatory, and fibrotic pathways, making it essential to identify novel targets that can address these different aspects. Advanced molecular profiling techniques, including transcriptomics, proteomics, metabolomics, and epigenomics, can provide valuable insights into the underlying mechanisms driving MASLD and guide the development of personalized treatment approaches.

AATF has been implicated in the pathogenesis of several cancers due to its role in the modulation of apoptotic pathways (19). We, for the first time, elucidated how TNF-α upregulates the expression of AATF via SREBP-1 and promotes hepatocarcinogenesis (35). Further studies revealed the role of AATF in impeding HCC angiogenesis by downregulating PEDF (24). Recently, we investigated the role of AATF in MASH-HCC and showed that TACE inhibition by Marimastat prevents AATF-mediated inflammation, fibrosis, and oncogenesis (27). In the current study, we identified for the first time the role of AATF in lipid metabolism and its implications in the development of MASH. The preclinical murine model of MASH used in this study is C57BL/6 mice fed with chow diet normal water and western diet sugar water that recapitulates the features of metabolic syndrome and MASH with progressive fibrosis, unlike the DIAMOND mouse model, which is a cross between two mouse strains (C57Bl/6J and 129S1/SvImJ) (36). The mice exhibit the development of fatty liver in 12 weeks after starting a western diet supplemented with sugar water, advancing to MASH and fibrosis at 24 weeks. Since AATF was found to be upregulated in both cellular and preclinical models of MASH, we evaluated the effect of liver-specific silencing of AATF against hepatic lipid accumulation in experimental MASH and its influence on the genes and proteins linked to the biological processes of MASH development and progression. The silencing of hepatic AATF showed a significant reduction in body weight and liver weight in WDSW mice and had no effect on CDNW mice. Insulin resistance was notably improved, and we also observed substantial improvement in both histological and biochemical parameters in WD siAATF mice compared to WDSW controls. Consistent with these data, AATF silencing also reduced fibrosis in the WDSW mice. These findings highlight the potential function of AATF in MASLD progression and set the stage for a deep dive into molecular insights.

This is the first study to have the hepatic metabolome performed in mice silenced with AATF. The mechanism by which AATF ameliorates MASH is elusive, and therefore high attention was paid to identifying the alterations in liver metabolites in the experimental MASH, where AATF was silenced versus the control by untargeted metabolomics. It was interesting to note the upregulation of glycerophospholipids, particularly phosphatidylcholines (PC), phosphatidylserines (PS), and phosphatidylethanolamines (PE), in the WD siAATF mice. Additionally, their breakdown products like LysoPC, LysoPS, and LysoPE were also increased. The metabolite-metabolite interaction network highlighted the potential functional relationships of glycerophospholipid with linoleate metabolism. It is noteworthy that alpha-linolenic acid (ALA), an essential omega-3 fatty acid, is largely attributed to its anti-inflammatory, antioxidant, and lipid-lowering properties in MASLD (37). ALA

can influence lipid metabolism by modulating the expression of genes involved in fatty acid oxidation and lipid synthesis. It also promotes the activation of peroxisome proliferator-activated receptors (PPARs), which play a crucial role in lipid metabolism (38).

Previous studies have also reported alterations in phospholipid content in the liver biopsies of NASH patients, suggesting that impaired phospholipid synthesis is associated with disease progression (13,14). The low hepatic phosphatidylcholine (PC) levels and the altered hepatic PC to phosphatidylethanolamine (PE) ratio appear to play significant roles in the development of MASLD (39). However, the pathophysiology of these lipid-induced processes remains not fully understood. Moreover, low PC levels have previously been shown to activate sterol regulatory element-binding protein 1 (SREBP1) (40). Essential phospholipids (EPLs) rich in phosphatidylcholine (PCH) are a widely used treatment option for fatty liver disease. There is substantial and consistent clinical evidence indicating that treatment with EPLs leads to the regression of steatosis (41). Studies show that phosphatidylcholine metabolism intersects with various metabolic pathways, and optimizing PC levels could potentially help regulate lipid metabolism and insulin sensitivity, thereby mitigating MASLD progression (42). In addition, PC may have antioxidant properties, which could counteract oxidative damage in the liver and protect against disease progression (43). Several classes of glycerophospholipids, such as PC, PE, PS, and PI, are implicated in MASLD progression, where dysregulation of these glycerophospholipids is linked with insulin, inflammation, and fibrosis, which are the hallmarks of MASLD (44). Consistent with this observation, we found that the markers of ER stress and inflammation were significantly reduced in AATF-silenced WD mice. Additionally, the liver metabolite profile in WD siAATF mice showed decreased branched-chain amino acid metabolism and sulfur metabolism involved in the MASH pathogenesis in contrast to increased pyruvate metabolism, NAD and FAD metabolism, as well as one-carbon metabolic pathways.

An intriguing observation in the current study using pathway enrichment analysis showed the mitochondrial beta-oxidation of the fatty acid pathway in the upregulated category along with phosphatidylcholine biosynthesis in WD siAATF mice. Corroborating these results, studies by Maev et al., have provided evidence that phosphatidylcholine supplementation may help improve liver function and reduce liver fat accumulation in fatty liver disease, potentially through its ability to activate PPARs and subsequent upregulation of PPAR-dependent enzymes, including acyl CoA oxidase and carnitine palmitoyl transferase (CPT), modulating lipid metabolism (45). Beta-oxidation helps to efficiently metabolize fatty acids, and thereby enhanced beta-oxidation may alleviate inflammation and oxidative stress in the liver, which are key drivers of MASLD progression (46). Several genes, such as CPT1 and PPARs, encode enzymes involved in beta-oxidation, and henceforth, upregulated expression of these genes would enhance beta-oxidation capacity, potentially improving metabolic health (47,48). Consistent with this, our study also showed the upregulation of CPT1, PPARα, and PPARγ genes in the liver tissue of WD siAATF compared to WD controls.

Despite the extensive studies on MASLD, there is a need to understand the interplay between the molecular drivers involved in lipid metabolism, insulin resistance, oxidative stress, and inflammation that contribute to the pathogenesis of MASLD.

This study offers insight for the first time on the involvement of AATF in fatty acid beta-oxidation, which plays a crucial role in the regulation of lipid metabolism and energy homeostasis in the liver. Thus, AATF is potentially a promising therapeutic target for the treatment of MASLD. Furthermore, studies are focused on elucidating the downstream interacting partners of AATF in fatty acid oxidation. An integrated transcriptomic and metabolomic analysis would aid in a better understanding of the role of AATF in the regulation of hepatic lipid metabolism.

ACKNOWLEDGMENT

This study was supported in whole or in part, by the SERB-POWER grant (SPG/2021/002524) and Ramalingaswami Re-entry Fellowship from the Department of Biotechnology (BT/RLF/Reentry/58/2017) to DPK, and Senior Research Fellowship (SRF) from ICMR to ANS.
The authors also acknowledge funding support from the Department of Biotechnology- Boost to University Interdisciplinary Life Science Departments for Education and Research programme (DBT-BUILDER: BT/INF/22/SP43045/2021) and the Department of Science and Technology–Promotion of University Research and Scientific Excellence (DST-PURSE) (SR/PURSE/2021/81 (c). The authors express sincere gratitude to the personnel of RGCB core facility (DBT-SAHAJ National Facility for Mass Spectrometry-Based Proteomics, Metabolomics and Lipidomics) for their technical assistance. We thank TheraCUES Innovations Pvt Ltd, Bangalore, India, for performing Bioinformatic analysis on the untargeted metabolomics assay data.

AUTHOR CONTRIBUTIONS

ANS and DPK conceptualized the project and designed the study; ANS and DS performed the experiments; ANS, DS, and DPK analyzed and interpreted the data; MM, ANS and GR analyzed metabolomics data; DS and PKS provided insights and reviewed the manuscript; ANS and DPK prepared the manuscript; DPK acquired funding and supervised the research. All authors read and approved the final version of the manuscript.

CONFLICTS OF INTEREST

The authors declare that there are no conflicts of interest.

REFERENCES

1. Younossi ZM, Golabi P, Paik JM, Henry A, Van Dongen C, Henry L. The global epidemiology of nonalcoholic fatty liver disease (NAFLD) and nonalcoholic steatohepatitis (NASH): a systematic review. Hepatology. 77(4) (2023) 1335-1347 doi:10.1097/HEP.0000000000000004.
2. Shalimar, Elhence A, Bansal B, Gupta H, Anand A, Singh TP, Goel A. Prevalence of Non-alcoholic Fatty Liver Disease in India: A Systematic Review and Meta-analysis. J Clin Exp Hepatol. May-Jun;12(3) (2022), 818-829. doi: 10.1016/j.jceh.2021.11.010
3. Paik JM, Golabi P, Younossi Y, Srishord M, Mishra A, Younossi ZM. The Growing Burden of Disability Related to Nonalcoholic Fatty Liver Disease: Data

From the Global Burden of Disease 2007-2017. Hepatol Commun. 4(12) (2020) 1769-1780. doi:10.1002/hep4.1599.

4. Suresh D, Srinivas AN, Kumar DP. Etiology of Hepatocellular Carcinoma: Special Focus on Fatty Liver Disease. Front Oncol. 30;10:601710. (2020) doi: 10.3389/fonc.2020.601710.
5. Chan WK, Chuah KH, Rajaram RB, Lim LL, Ratnasingam J, Vethakkan SR. Metabolic Dysfunction-Associated Steatotic Liver Disease (MASLD): A State-of-the-Art Review. J Obes Metab Syndr. 2023 Sep 30;32(3):197-213. doi: 10.7570/jomes23052.
6. Byrne CD, Targher G. NAFLD: a multisystem disease. J Hepatol. 2015 Apr;62(1 Suppl):S47-64. doi: 10.1016/j.jhep.2014.12.012.
7. Llovet JM, Willoughby CE, Singal AG, Greten TF, Heikenwälder M, El-Serag HB, Finn RS, Friedman SL. Nonalcoholic steatohepatitis-related hepatocellular carcinoma: pathogenesis and treatment. Nat Rev Gastroenterol Hepatol. 2023 Aug;20(8):487-503. doi: 10.1038/s41575-023-00754-7.
8. Duseja A, Singh SP, De A, Madan K, Rao PN, Shukla A, Choudhuri G, Saigal S, Shalimar, Arora A, Anand AC, Das A, Kumar A, Eapen CE, Devadas K, Shenoy KT, Panigrahi M, Wadhawan M, Rathi M, Kumar M, Choudhary NS, Saraf N, Nath P, Kar S, Alam S, Shah S, Nijhawan S, Acharya SK, Aggarwal V, Saraswat VA, Chawla YK. Indian National Association for Study of the Liver (INASL) Guidance Paper on Nomenclature, Diagnosis and Treatment of Nonalcoholic Fatty Liver Disease (NAFLD). J Clin Exp Hepatol. 13(2) (2023), 273-302. doi: 10.1016/j.jceh.2022.11.014.
9. Li Y, Yang P, Ye J, Xu Q, Wu J, Wang Y. Updated mechanisms of MASLD pathogenesis. Lipids Health Dis. 2024 Apr 22;23(1):117. doi: 10.1186/s12944-024-02108-x.
10. Rao G, Peng X, Li X, An K, He H, Fu X, Li S, An Z. Unmasking the enigma of lipid metabolism in metabolic dysfunction-associated steatotic liver disease: from mechanism to the clinic. Front Med (Lausanne). 2023 Nov 27;10:1294267. doi: 10.3389/fmed.2023.1294267
11. Venkatesan N, Doskey LC, Malhi H. The Role of Endoplasmic Reticulum in Lipotoxicity during Metabolic Dysfunction-Associated Steatotic Liver Disease (MASLD) Pathogenesis. Am J Pathol. 2023 Dec;193(12):1887-1899. doi: 10.1016/j.ajpath.2023.08.007.
12. Syed-Abdul MM. Lipid Metabolism in Metabolic-Associated Steatotic Liver Disease (MASLD). Metabolites. 2023 Dec 23;14(1):12. doi: 10.3390/metabo14010012.
13. Puri P, Baillie RA, Wiest MM, Mirshahi F, Choudhury J, Cheung O, Sargeant C, Contos MJ, Sanyal AJ. A lipidomic analysis of nonalcoholic fatty liver disease. Hepatology 2007; 46: 1081-1090 DOI: 10.1002/hep.21763
14. Chiappini F, Coilly A, Kadar H, Gual P, Tran A, Desterke C, Samuel D, Duclos-Vallée JC, Touboul D, Bertrand-Michel J, Brunelle A, Guettier C, Le Naour F.

Metabolism dysregulation induces a specific lipid signature of nonalcoholic steatohepatitis in patients. Sci Rep 2017; 7: 46658. doi:10.1038/srep46658

15. Marc Prentki, S. R. Murthy Madiraju, Glycerolipid Metabolism and Signaling in Health and Disease, Endocrine Reviews, Volume 29, Issue 6, 1 October 2008, Pages 647–676, https://doi.org/10.1210/er.2008-0007
16. Chen H, Tan H, Wan J, Zeng Y, Wang J, Wang H, Lu X. PPAR-γ signaling in nonalcoholic fatty liver disease: Pathogenesis and therapeutic targets. Pharmacol Ther. 2023 May;245:108391. doi: 10.1016/j.pharmthera.2023.108391.
17. Tong L, Wang L, Yao S, Jin L, Yang J, Zhang Y, Ning G, Zhang Z. PPARδ attenuates hepatic steatosis through autophagy-mediated fatty acid oxidation. Cell Death Dis. 2019 Feb 27;10(3):197. doi: 10.1038/s41419-019-1458-8.
18. Weber M, Mera P, Casas J, Salvador J, Rodríguez A, Alonso S, Sebastián D, Soler-Vázquez MC, Montironi C, Recalde S, Fucho R, Calderón-Domínguez M, Mir JF, Bartrons R, Escola-Gil JC, Sánchez-Infantes D, Zorzano A, Llorente-Cortes V, Casals N, Valentí V, Frühbeck G, Herrero L, Serra D. Liver CPT1A gene therapy reduces diet-induced hepatic steatosis in mice and highlights potential lipid biomarkers for human NAFLD. FASEB J. 2020 Sep;34(9):11816-11837. doi: 10.1096/fj.202000678R.
19. Srinivas AN, Suresh D, Mirshahi F, Santhekadur PK, Sanyal AJ, Kumar DP. Emerging roles of AATF: Checkpoint signaling and beyond. J Cell Physiol. 2021 May;236(5):3383-3395. doi: 10.1002/jcp.30141.
20. Iezzi S, Fanciulli M. Discovering Che-1/AATF: a new attractive target for cancer therapy. Front Genet. 2015 Apr 10;6:141. doi: 10.3389/fgene.2015.00141.
21. Jackson JG, Lozano G. Che-ating death: CHE1/AATF protects from p53-mediated apoptosis. EMBO J. 2012 Oct 17;31(20):3951-3. doi: 10.1038/emboj.2012.258.
22. Welcker D, Jain M, Khurshid S, Jokić M, Höhne M, Schmitt A, Frommolt P, Niessen CM, Spiro J, Persigehl T, Wittersheim M, Büttner R, Fanciulli M, Schermer B, Reinhardt HC, Benzing T, Höpker K. AATF suppresses apoptosis, promotes proliferation and is critical for Kras-driven lung cancer. Oncogene. 2018 Mar;37(11):1503-1518. doi: 10.1038/s41388-017-0054-6.
23. Haanpää M, Reiman M, Nikkilä J, Erkko H, Pylkäs K, Winqvist R. Mutation analysis of the AATF gene in breast cancer families. BMC Cancer. 2009 Dec 21;9:457. doi: 10.1186/1471-2407-9-457.
24. Kaul D, Mehrotra A. Functional characterization of AATF transcriptome in human leukemic cells. Mol Cell Biochem. 2007 Mar;297(1-2):215-20. doi: 10.1007/s11010-006-9317-1.
25. Suresh D, Srinivas AN, Prashant A, Satish S, Vishwanath P, Nataraj SM, Koduru SV, Santhekadur PK, Kumar DP. AATF inhibition exerts antiangiogenic effects against human hepatocellular carcinoma. Front Oncol. 2023 Jun 9;13:1130380. doi: 10.3389/fonc.2023.1130380.

26. Srinivas AN, Suresh D, Chidambaram SB, Santhekadur PK, Kumar DP. Apoptosis antagonizing transcription factor-mediated liver damage and inflammation to cancer: Therapeutic intervention by curcumin in experimental metabolic dysfunction associated steatohepatitis-hepatocellular carcinoma. J Cell Physiol. 2024 Jan;239(1):135-151. doi: 10.1002/jcp.31151.

27. Srinivas AN, Suresh D, Vishwanath PM, Satish S, Santhekadur PK, Koka S, Kumar DP. TACE inhibition: a promising therapeutic intervention against AATF-mediated steatohepatitis to hepatocarcinogenesis. Mol Oncol. 2024 Apr 1. doi: 10.1002/1878-0261.13646.

28. Srinivas AN, Suresh D, Suvarna D, Pathak P, Giri S, Suman, Satish S, Chidambaram SB, Kumar DP. Unraveling the Potential Role of Tecomella undulata in Experimental NASH. Int J Mol Sci. 2023 Feb 7;24(4):3244. doi: 10.3390/ijms24043244.

29. Banini BA, Kumar DP, Cazanave S, Seneshaw M, Mirshahi F, Santhekadur PK, Wang L, Guan HP, Oseini AM, Alonso C, Bedossa P, Koduru SV, Min HK, Sanyal AJ. Identification of a Metabolic, Transcriptomic, and Molecular Signature of Patatin-Like Phospholipase Domain Containing 3-Mediated Acceleration of Steatohepatitis. Hepatology. doi: 10.1002/hep.31609.

30. Liu Z, Wang P, Liu Z, Wei C, Li Y, Liu L. Evaluation of liver tissue extraction protocol for untargeted metabolomics analysis by ultra-high-performance liquid chromatography/tandem mass spectrometry. J Sep Sci. 2021 Sep;44(18):3450-3461. doi: 10.1002/jssc.202100051

31. Han J, Kaufman RJ. The role of ER stress in lipid metabolism and lipotoxicity. J Lipid Res. 2016 Aug;57(8):1329-38. doi: 10.1194/jlr.R067595.

32. Dempsey JL, Ioannou GN, Carr RM. Mechanisms of Lipid Droplet Accumulation in Steatotic Liver Diseases. Semin Liver Dis. 2023 Nov;43(4):367-382. doi: 10.1055/a-2186-3557.

33. Perry RJ, Samuel VT, Petersen KF, Shulman GI. The role of hepatic lipids in hepatic insulin resistance and type 2 diabetes. Nature. 2014 Jun 5;510(7503):84-91. doi: 10.1038/nature13478.

34. Duan Y, Pan X, Luo J, Xiao X, Li J, Bestman PL, Luo M. Association of Inflammatory Cytokines With Non-Alcoholic Fatty Liver Disease. Front Immunol. 2022 May 6;13:880298. doi: 10.3389/fimmu.2022.880298.

35. Kumar DP, Santhekadur PK, Seneshaw M, Mirshahi F, Uram-Tuculescu C, Sanyal AJ. A Regulatory Role of Apoptosis Antagonizing Transcription Factor in the Pathogenesis of Nonalcoholic Fatty Liver Disease and Hepatocellular Carcinoma. Hepatology. 2019 Apr;69(4):1520-1534. doi: 10.1002/hep.30346.

36. Asgharpour A, Cazanave SC, Pacana T, Seneshaw M, Vincent R, Banini BA, Kumar DP, Daita K, Min HK, Mirshahi F, Bedossa P, Sun X, Hoshida Y, Koduru SV, Contaifer D Jr, Warncke UO, Wijesinghe DS, Sanyal AJ. A diet-induced animal model of non-alcoholic fatty liver disease and hepatocellular cancer. J Hepatol. 2016 Sep;65(3):579-88. doi: 10.1016/j.jhep.2016.05.005.

37. Jordão Candido C, Silva Figueiredo P, Del Ciampo Silva R, et al. Protective Effect of α-Linolenic Acid on Non-Alcoholic Hepatic Steatosis and Interleukin-6 and -10 in Wistar Rats. Nutrients. 2019;12(1):9. doi:10.3390/nu12010009

38. Yang L, Yuan J, Liu L, Shi C, Wang L, Tian F, Liu F, Wang H, Shao C, Zhang Q, Chen Z, Qin W, Wen W. α-linolenic acid inhibits human renal cell carcinoma cell proliferation through PPAR-γ activation and COX-2 inhibition. Oncol Lett. 2013 Jul;6(1):197-202. doi: 10.3892/ol.2013.1336.

39. Arendt BM, Ma DW, Simons B, Noureldin SA, Therapondos G, Guindi M, Sherman M, Allard JP. Nonalcoholic fatty liver disease is associated with lower hepatic and erythrocyte ratios of phosphatidylcholine to phosphatidylethanolamine. Appl Physiol Nutr Metab. 2013 Mar;38(3):334-40. doi: 10.1139/apnm-2012-0261.

40. Walker AK, Jacobs RL, Watts JL, Rottiers V, Jiang K, Finnegan DM, Shioda T, Hansen M, Yang F, Niebergall LJ, Vance DE, Tzoneva M, Hart AC, Näär AM. A conserved SREBP-1/phosphatidylcholine feedback circuit regulates lipogenesis in metazoans. Cell. 2011 Nov 11;147(4):840-52. doi: 10.1016/j.cell.2011.09.045.

41. Dajani AI, Popovic B. Essential phospholipids for nonalcoholic fatty liver disease associated with metabolic syndrome: A systematic review and network meta-analysis. World J Clin Cases. 2020;8(21):5235-5249. doi:10.12998/wjcc.v8.i21.5235

42. Osipova D, Kokoreva K, Lazebnik L, Golovanova E, Pavlov C, Dukhanin A, Orlova S, Starostin K. Regression of Liver Steatosis Following Phosphatidylcholine Administration: A Review of Molecular and Metabolic Pathways Involved. Front Pharmacol. 2022 Mar 10;13:797923. doi: 10.3389/fphar.2022.797923.

43. Maev IV, Samsonov AA, Palgova LK, et al. Effectiveness of phosphatidylcholine in alleviating steatosis in patients with non-alcoholic fatty liver disease and cardiometabolic comorbidities (MANPOWER study). BMJ Open Gastroenterol. 2020;7(1):e000341. Published 2020 Jan 13. doi:10.1136/bmjgast-2019-000341

44. Cohn, J. S., Wat, E., Kamili, A., and Tandy, S. (2008). Dietary Phospholipids, Hepatic Lipid Metabolism and Cardiovascular Disease. Curr. Opin. Lipidol. 19, 257–262. doi:10.1097/MOL.0b013e3282ffaf96

45. Maev IV, Samsonov AA, Palgova LK, Pavlov CS, Shirokova EN, Vovk EI, Starostin KM. Effectiveness of phosphatidylcholine as adjunctive therapy in improving liver function tests in patients with non-alcoholic fatty liver disease and metabolic comorbidities: real-life observational study from Russia. BMJ Open Gastroenterol. 2020 Mar 26;7(1):e000368. doi: 10.1136/bmjgast-2019-000368.

46. Ipsen DH, Lykkesfeldt J, Tveden-Nyborg P. Molecular mechanisms of hep2021 Apr;73(4):1290-1306. atic lipid accumulation in non-alcoholic fatty liver disease. Cell Mol Life Sci. 2018;75(18):3313-3327. doi:10.1007/s00018-018-2860-6

47. Fondevila MF, Fernandez U, Heras V, Parracho T, Gonzalez-Rellan MJ, Novoa E, Porteiro B, Alonso C, Mayo R, da Silva Lima N, Iglesias C, Filliol AA, Senra

A, Delgado TC, Woodhoo A, Herrero L, Serra D, Prevot V, Schwaninger M, López M, Dieguez C, Millet O, Mato JM, Cubero FJ, Varela-Rey M, Iruzubieta P, Crespo J, Martinez-Chantar ML, Schwabe RF, Nogueiras R. Inhibition of carnitine palmitoyltransferase 1A in hepatic stellate cells protects against fibrosis. J Hepatol. 2022 Jul;77(1):15-28. doi: 10.1016/j.jhep.2022.02.003.

48. Régnier M, Polizzi A, Smati S, Lukowicz C, Fougerat A, Lippi Y, Fouché E, Lasserre F, Naylies C, Bétoulières C, Barquissau V, Mouisel E, Bertrand-Michel J, Batut A, Saati TA, Canlet C, Tremblay-Franco M, Ellero-Simatos S, Langin D, Postic C, Wahli W, Loiseau N, Guillou H, Montagner A. Hepatocyte-specific deletion of Pparα promotes NAFLD in the context of obesity. Sci Rep. 2020 Apr 16;10(1):6489. doi: 10.1038/s41598-020-63579-3.

FIGURE LEGENDS

Figure 1. AATF is upregulated in the *in vitro* and *in vivo* MASH models
HepG2 and Huh7 cells were treated with 0.5mM of SP, SO, or SP+SO for 24 hours. Lipid accumulation was determined by Oil Red O staining (A). The mRNA expression of AATF in HepG2 (B) and Huh7 (C) cells. Protein levels of AATF in HepG2 and Huh7 cells (D). Diet-induced MASH model was developed by feeding the mice with chow diet normal water (CDNW) or western diet sugar water (WDSW) for 24 weeks. Representative H&E images and AATF immunohistochemistry of control, MAFL, and MASH stages (E). hepatic AATF mRNA (F) and protein (G) levels were evaluated in mice liver tissue. All the data are expressed as mean±SEM for 6-8 mice per group. Statistical significance was analyzed by a student's t-test. **$p<0.001$ or *$P < 0.05$ compared to normal or control.

Figure 2. Hepatocyte-specific knockdown of AATF improves metabolic health
C57Bl/6 mice were fed chow diet normal water or western diet sugar water for 12 weeks. Liver-specific AAV8-TBG-Null or AAV8-TBG-siAATF vectors were injected via tail vein into mice and monitored for an additional 12 weeks (A). Tissue distribution of vector (B), liver-specific (C), and hepatocyte-specific (D) of AATF silencing were determined. Body weight (E), liver weight (F), liver-body ratio (G), and adipose tissue weight (H) were determined. Glucose tolerance test (I) and insulin tolerance test (J) were performed. All the data are expressed as mean±SEM for 6-8 mice per group. Statistical significance was analyzed by a student's t-test. $^{\#\#}p<0.001$ compared to CD control; **$p<0.001$ compared to WD control or AAV8 control.

Figure 3. Hepatocyte-specific knockdown of AATF improves liver injury and impaired lipid metabolism
Mice were euthanized after 24 weeks and blood was collected. Fasting blood glucose (A), fasting insulin (B), and HOMA-IR (C) were determined. Serum levels of ALT (D), AST (E), total cholesterol (F), triglycerides (G), and LDL-cholesterol (H) were measured. Representative gross liver images (I), H&E staining (J), and Oil Red O staining (K). Data expressed as mean ±SEM for 6-8 mice. Statistical significance was analyzed by a student's t-test. $^{\#\#}p<0.001$ compared to CD control; **$p<0.001$ compared to WD control.

Figure 4. Silencing of AATF ameliorates MASH and liver fibrosis

Histology scores were calculated for mice liver sections. Representative images and scoring of steatosis (A), lobular inflammation (B), hepatocyte ballooning (C), and MASLD activity score (D). Representative images of picrosirius red staining and fibrosis scoring (E), immunostaining of desmin with scoring (F). Hepatic mRNA expression of Col1A1 (G), Col3A1 (H), α-SMA (I), and TGF-β (J) quantified. Data expressed as mean ±SEM for 6-8 mice. Statistical significance was analyzed by a student's t-test. $^{##}p<0.001$ or $^{#}p<0.05$ compared to CD control; $^{**}p<0.001$ compared to WD control.

Figure 5. Effect of silencing AATF on ER stress and Inflammation in Experimental MASH

C57Bl/6 mice were fed chow diet normal water (CD) or western diet sugar water (WD) for 12 weeks. Liver-specific AAV8-TBG-Null or AAV8-TBG-siAATF vectors were injected via tail vein into mice and monitored for an additional 12 weeks. (A-D) hepatic mRNA expression of ER stress markers- CHOP, Grp78, PERK, and ATF4, (E-G) hepatic mRNA expression of inflammatory markers- IL-1β, IL-6, and TNF-α, (H) serum TNF- α by ELISA. (I and J) Liver tissue lysates were used for immunoblotting of inflammatory markers- pJNK and pERK1/2. (K) F4/80 staining. Data expressed as mean ±SEM for 6-8 mice. Statistical significance was analyzed by a student's t-test. $^{##}p<0.001$ or $^{#}p<0.05$ compared to CD control; $^{**}p<0.001$ or $^{*}p<0.05$ compared to WD control.

Figure 6. Effect of AATF silencing on hepatic metabolites in experimental MASH

C57Bl/6 mice were fed chow diet normal water (CD) or western diet sugar water (WD) for 12 weeks. Liver-specific AAV8-TBG-blank (C) or AAV8-TBG-siAATF (siAATF) vectors were injected via tail vein into mice and monitored for an additional 12 weeks. After mice were euthanized, liver tissues were collected for untargeted metabolomic study. (A) PCA score plot (B) PLS-DA plot among the four groups showing a clear group separation between the groups, (C) Classification of differential metabolites between the four groups, (D) Venn diagram showing the up and downregulated metabolites between the WDC vs. CDC and WDsiAATF vs. WDC. Volcano plot for differential metabolites in WDC vs. CDC (E) and WDsiAATF vs. WDC (F).

Figure 7. Hepatic silencing of AATF increases glycerophospholipid synthesis in MASH mice

C57Bl/6 mice were fed chow diet normal water (CD) or western diet sugar water (WD) for 12 weeks. Liver-specific AAV8-TBG-Null (C) or AAV8-TBG-siAATF (siAATF) vectors were injected via tail vein into mice and monitored for an additional 12 weeks. Untargeted metabolomics was carried out in mice liver tissues. Bubble plot showing top 20 KEGG pathways enrichment using the mummichog GSEA algorithm in (A) WDC vs. CDC and (B) WDC vs. WDsiAATF. A bubble plot showing lipid superclass (C) and lipid subclass (D) enrichment using the mummichog GSEA algorithm. (E) Heat map of different glycerophospholipids differentially altered between WDC and WDsiAATF mice.

Figure 8. Metabolic networking of glycerophospholipid metabolism

Untargeted metabolomics was carried out in mice liver tissues. Metabolites of glycerophospholipid metabolism were analyzed and functional correlation network

analysis was carried out. (A) Glycerophospholipid metabolism pathway visualized in pathview network highlighting the dysregulated compounds (up/downregulated) in WDsiAATF vs. WDC. (B) Relative abundance of phosphocholine, PC (phosphatidylcholine), LPE (lysophophatidylethanolamine), and LPC (lysophosphatidylcholine). (C) Metabolite functional interaction network of glycerophospholipid metabolism pathway. Statistical significance was analyzed by a student's t-test. **p<0.001 or *p<0.05 compared to WDC.

Figure 9. AATF knockdown promotes β oxidation of fatty acids in MASH mice
Untargeted metabolomics was carried out in mice liver tissues. Pathway analysis and enrichment analysis of metabolomic data were carried out. Enrichment analysis based on the Small Molecule Pathway Database (SMPDB) was performed (A) Up regulated pathways (B) downregulated pathways. (C) hepatic mRNA expression of mitochondrial β oxidation genes (CPT-1α, PGC-1α, PPAR-α, and PPAR-γ). Data expressed as mean ±SEM. Statistical significance was analyzed by a student's t-test. **P < 0.001 or *P < 0.05 compared to WDC. (D) Schematic representation depicting how hepatic silencing of AATF ameliorates MASH by promoting β oxidation of fatty acids.

Figure 1

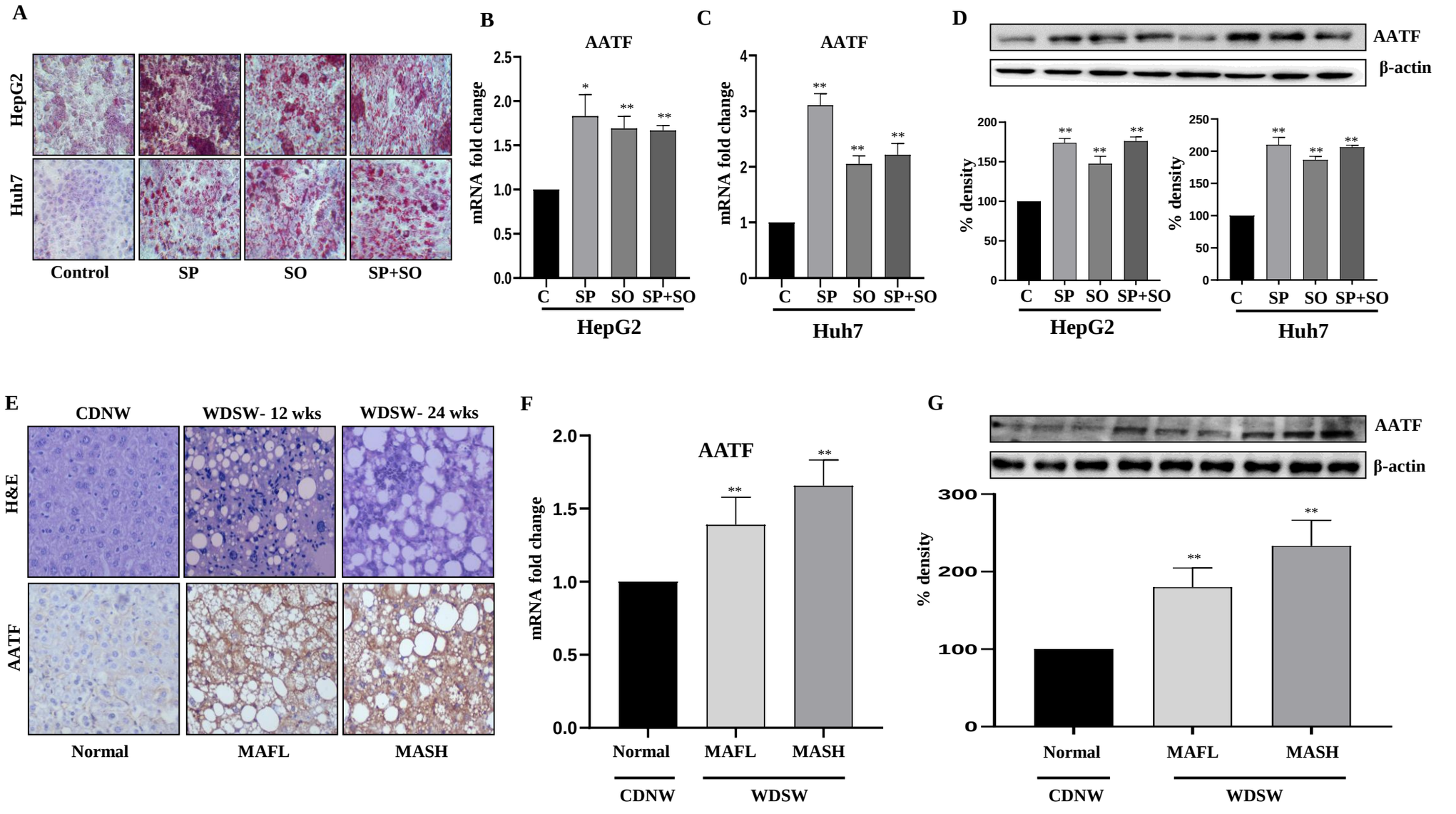
A
HepG2
Huh7
Control
SP
SO
SP+SO
B
AATF
mRNA fold change
C
SP
SO
SP+SO
HepG2
C
AATF
mRNA fold change
Huh7
D
AATF
β-actin
% density
HepG2
Huh7
E
CDNW
WDSW- 12 wks
WDSW- 24 wks
H&E
AATF
Normal
MAFL
MASH
F
AATF
mRNA fold change
Normal
MAFL
MASH
CDNW
WDSW
G
AATF
β-actin
% density
Normal
MAFL
MASH
CDNW
WDSW

Figure 2

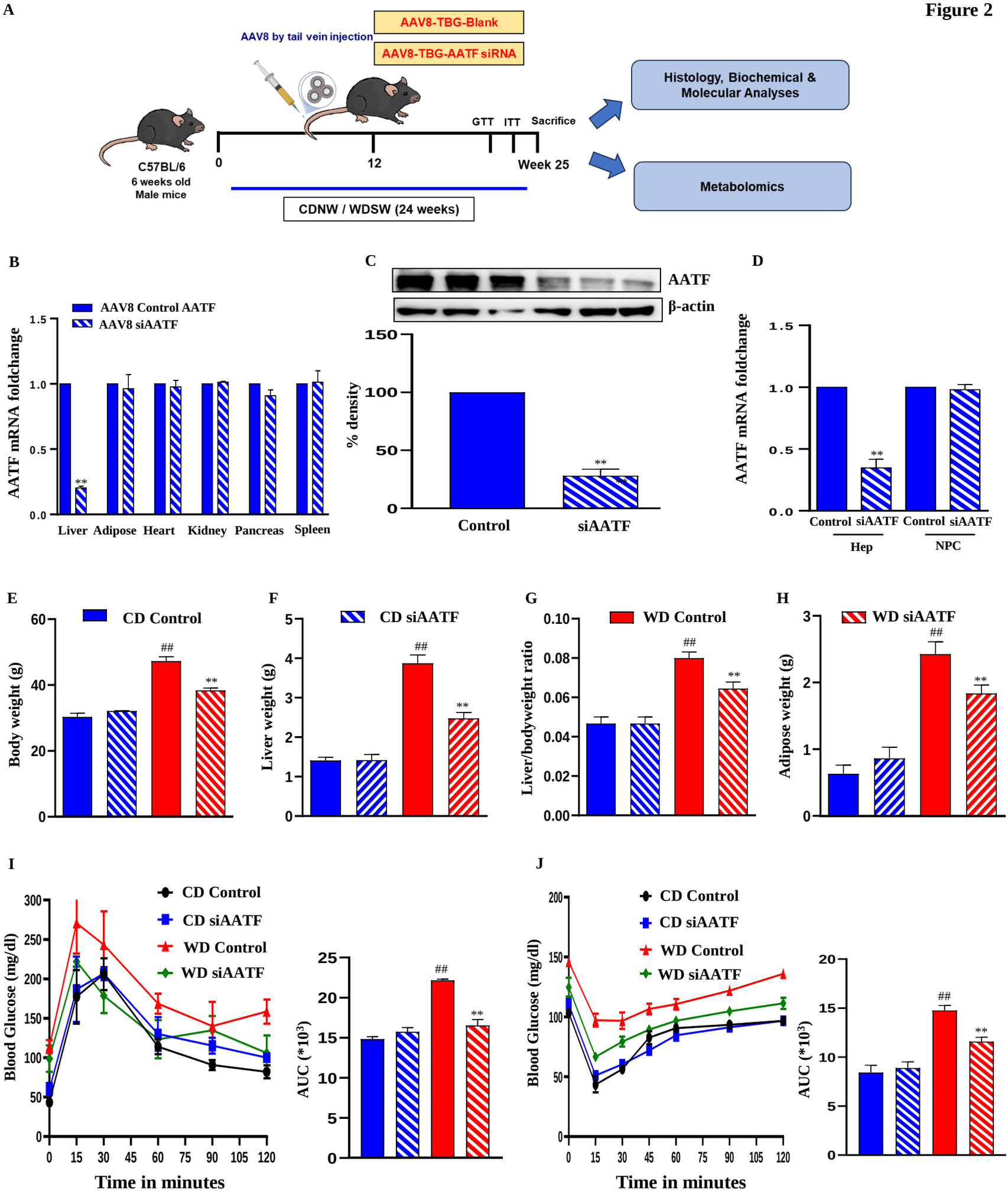
A
AAV8 by tail vein injection
AAV8-TBG-Blank
AAV8-TBG-AATF siRNA
C57BL/6
6 weeks old
Male mice
0
12
GTT
ITT
Sacrifice
Week 25
CDNW / WDSW (24 weeks)
Histology, Biochemical & Molecular Analyses
Metabolomics
B
AAV8 Control AATF
AAV8 siAATF
AATF mRNA foldchange
Liver
Adipose
Heart
Kidney
Pancreas
Spleen
C
AATF
β-actin
% density
Control
siAATF
D
AATF mRNA foldchange
Control
siAATF
Control
siAATF
Hep
NPC
E
CD Control
Body weight (g)
F
CD siAATF
Liver weight (g)
G
WD Control
Liver/bodyweight ratio
H
WD siAATF
Adipose weight (g)
I
CD Control
CD siAATF
WD Control
WD siAATF
Blood Glucose (mg/dl)
Time in minutes
AUC (*10³)
J
CD Control
CD siAATF
WD Control
WD siAATF
Blood Glucose (mg/dl)
Time in minutes
AUC (*10³)

Figure 3

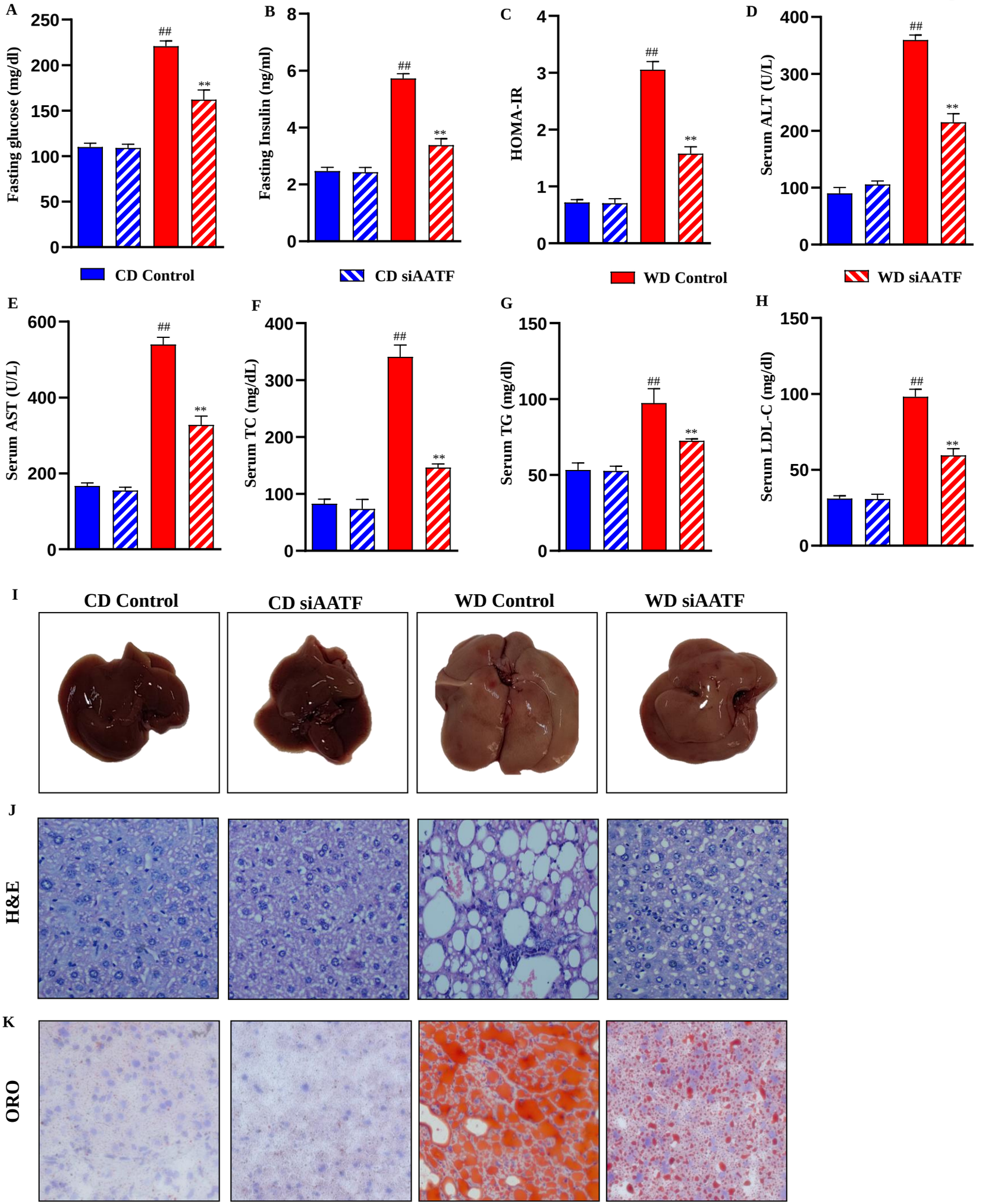
A
Fasting glucose (mg/dl)
250
200
150
100
50
0
##
**
B
Fasting Insulin (ng/ml)
8
6
4
2
0
##
**
C
HOMA-IR
4
3
2
1
0
##
**
D
Serum ALT (U/L)
400
300
200
100
0
##
**
CD Control
CD siAATF
WD Control
WD siAATF
E
Serum AST (U/L)
600
400
200
0
##
**
F
Serum TC (mg/dL)
400
300
200
100
0
##
**
G
Serum TG (mg/dl)
150
100
50
0
##
**
H
Serum LDL-C (mg/dl)
150
100
50
0
##
**
I
CD Control
CD siAATF
WD Control
WD siAATF
J
H&E
K
ORO

Figure 4

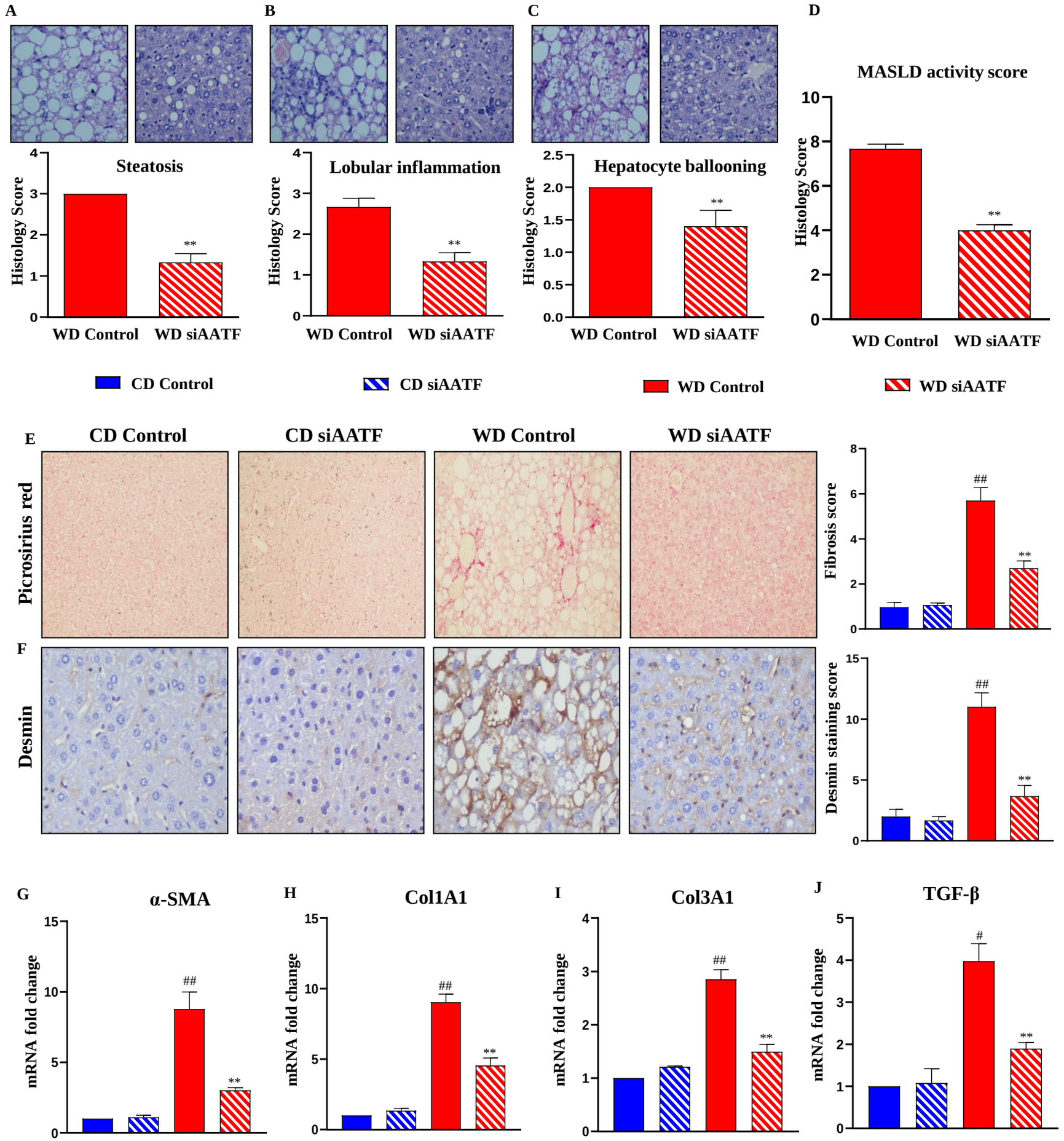
A
B
C
D
Steatosis
Lobular inflammation
Hepatocyte ballooning
MASLD activity score
Histology Score
WD Control
WD siAATF
CD Control
CD siAATF
E
F
Picrosirius red
Desmin
Fibrosis score
Desmin staining score
G
H
I
J
α-SMA
Col1A1
Col3A1
TGF-β
mRNA fold change

Figure 5

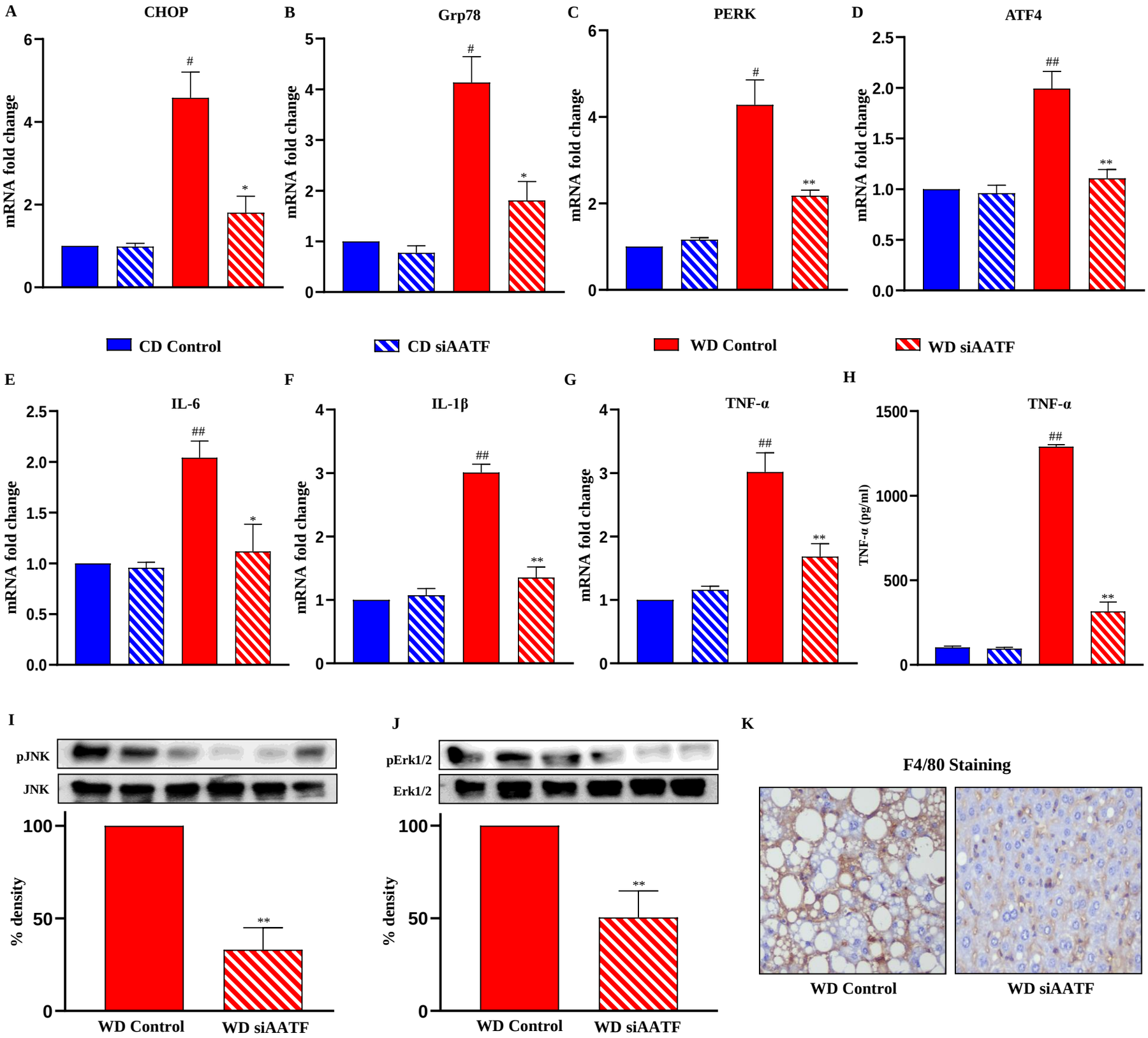
A
CHOP
mRNA fold change
B
Grp78
C
PERK
D
ATF4
CD Control
CD siAATF
WD Control
WD siAATF
E
IL-6
F
IL-1β
G
TNF-α
H
TNF-α
TNF-α (pg/ml)
I
pJNK
JNK
% density
WD Control
WD siAATF
J
pErk1/2
Erk1/2
K
F4/80 Staining

Figure 6

A

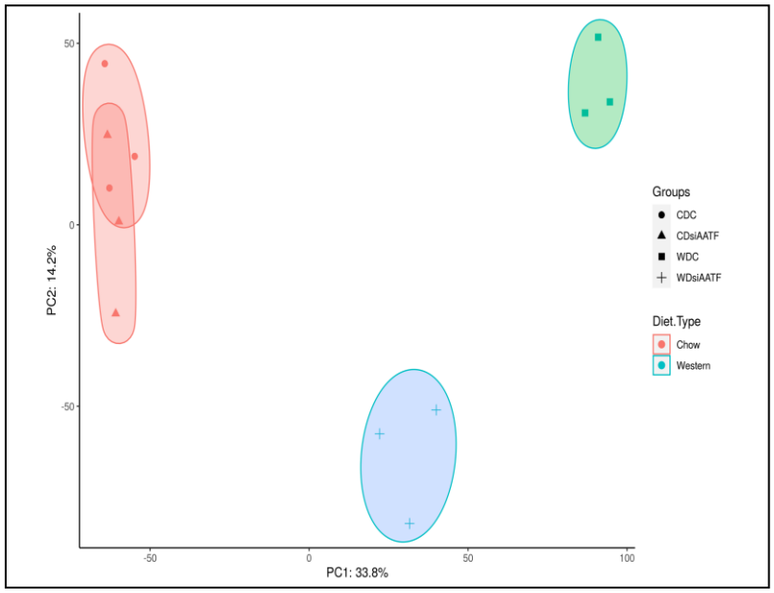

B

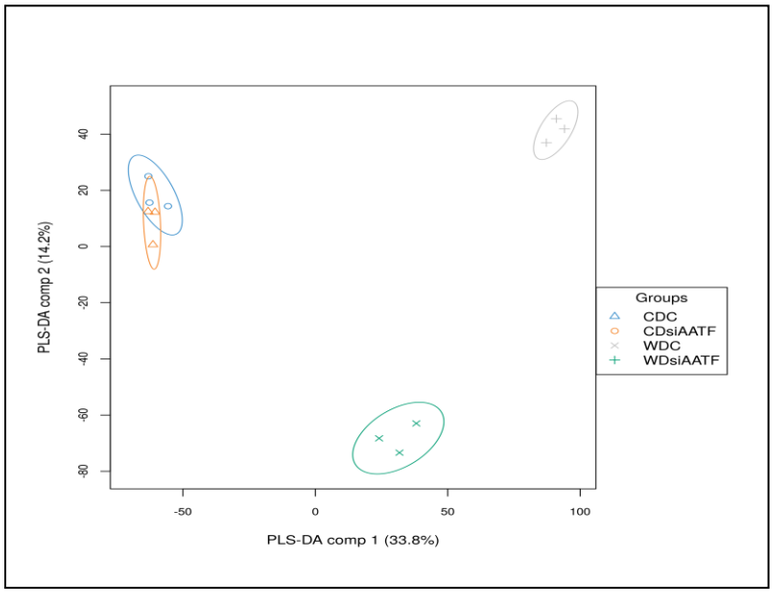

C

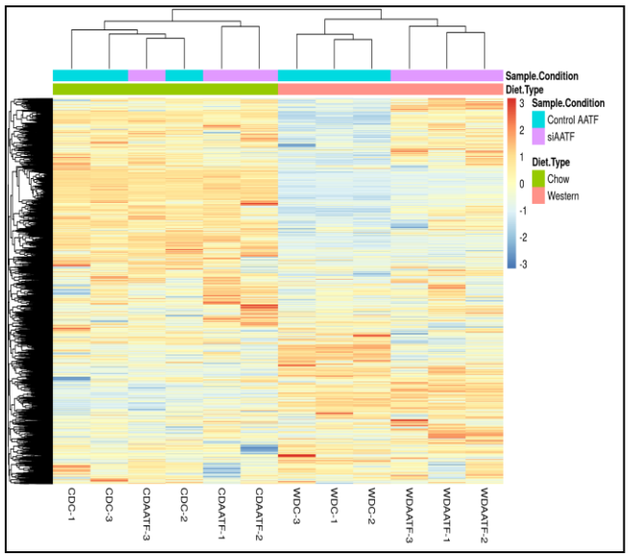

D

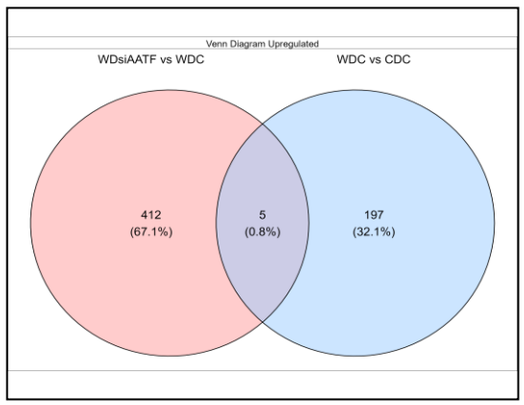

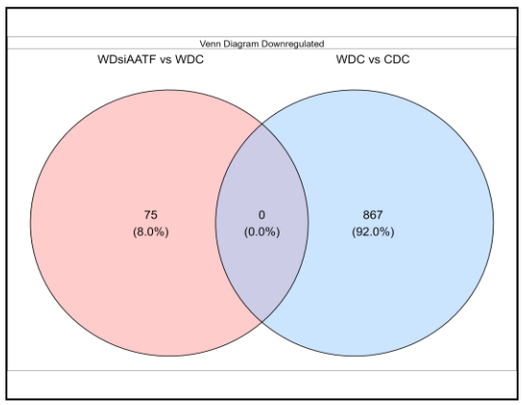

E

F

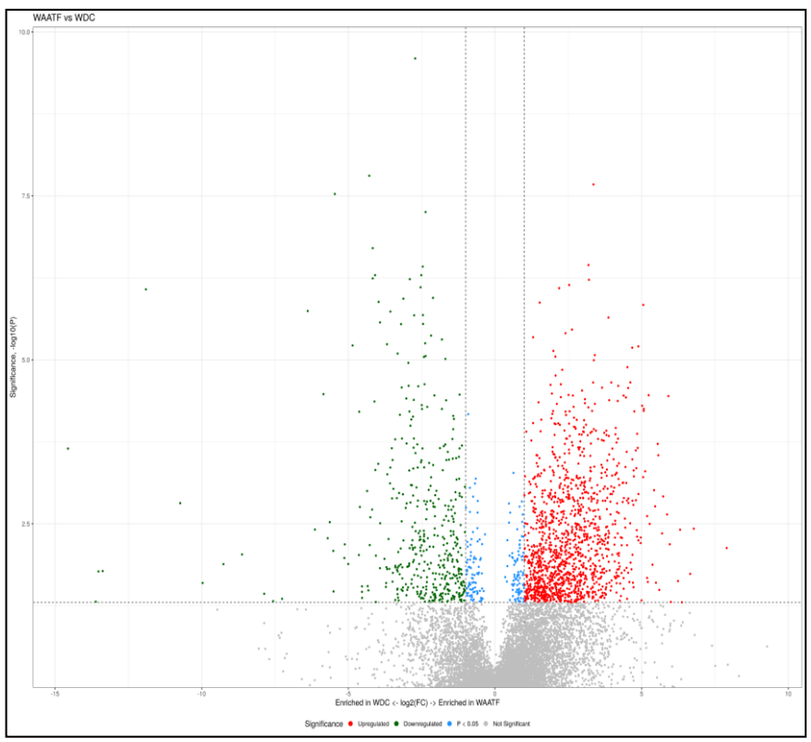

Figure 7

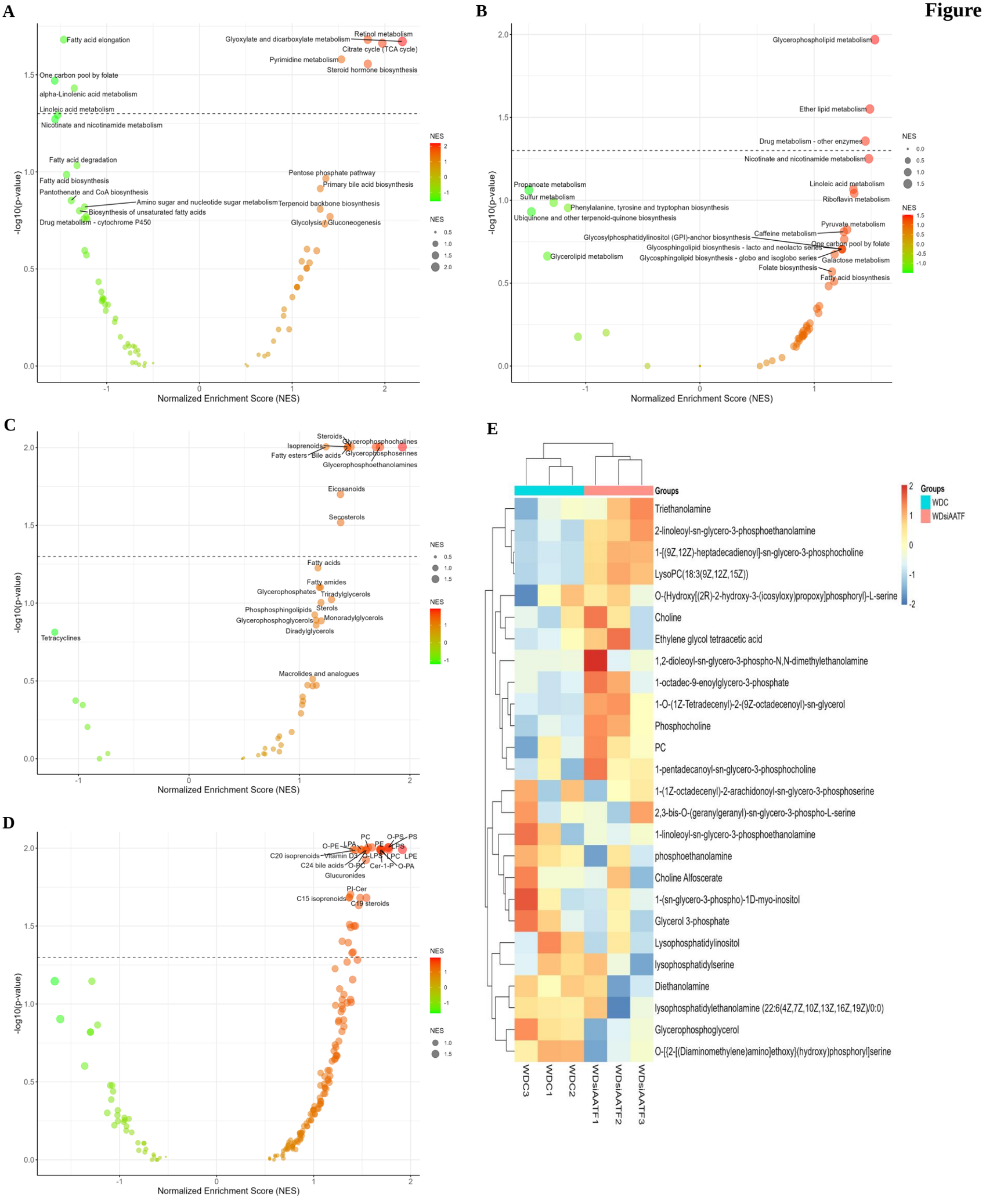
A
Fatty acid elongation
Glyoxylate and dicarboxylate metabolism
Retinol metabolism
Citrate cycle (TCA cycle)
Pyrimidine metabolism
Steroid hormone biosynthesis
One carbon pool by folate
alpha-Linolenic acid metabolism
Linoleic acid metabolism
Nicotinate and nicotinamide metabolism
Fatty acid degradation
Fatty acid biosynthesis
Pantothenate and CoA biosynthesis
Amino sugar and nucleotide sugar metabolism
Biosynthesis of unsaturated fatty acids
Drug metabolism - cytochrome P450
Pentose phosphate pathway
Primary bile acid biosynthesis
Terpenoid backbone biosynthesis
Glycolysis / Gluconeogenesis
-log10(p-value)
Normalized Enrichment Score (NES)
NES
B
Glycerophospholipid metabolism
Ether lipid metabolism
Drug metabolism - other enzymes
Nicotinate and nicotinamide metabolism
Propanoate metabolism
Sulfur metabolism
Phenylalanine, tyrosine and tryptophan biosynthesis
Ubiquinone and other terpenoid-quinone biosynthesis
Linoleic acid metabolism
Riboflavin metabolism
Pyruvate metabolism
Caffeine metabolism
Glycosylphosphatidylinositol (GPI)-anchor biosynthesis
Glycosphingolipid biosynthesis - lacto and neolacto series
One carbon pool by folate
Glycosphingolipid biosynthesis - globo and isoglobo series
Galactose metabolism
Folate biosynthesis
Fatty acid biosynthesis
Glycerolipid metabolism
C
Steroids
Isoprenoids
Fatty esters
Bile acids
Glycerophosphocholines
Glycerophosphoserines
Glycerophosphoethanolamines
Eicosanoids
Secosterols
Fatty acids
Fatty amides
Glycerophosphates
Triradylglycerols
Phosphosphingolipids
Sterols
Glycerophosphoglycerols
Monoradylglycerols
Diradylglycerols
Tetracyclines
Macrolides and analogues
D
PC
O-PS
PS
O-PE
LPA
PE
LPS
C20 isoprenoids
Vitamin D3
O-LPS
LPC
LPE
C24 bile acids
O-PC
Cer-1-P
O-PA
Glucuronides
PI-Cer
C15 isoprenoids
C19 steroids
E
Groups
WDC
WDsiAATF
Triethanolamine
2-linoleoyl-sn-glycero-3-phosphoethanolamine
1-[(9Z,12Z)-heptadecadienoyl]-sn-glycero-3-phosphocholine
LysoPC(18:3(9Z,12Z,15Z))
O-{Hydroxy[(2R)-2-hydroxy-3-(icosyloxy)propoxy]phosphoryl}-L-serine
Choline
Ethylene glycol tetraacetic acid
1,2-dioleoyl-sn-glycero-3-phospho-N,N-dimethylethanolamine
1-octadec-9-enoylglycero-3-phosphate
1-O-(1Z-Tetradecenyl)-2-(9Z-octadecenoyl)-sn-glycerol
Phosphocholine
PC
1-pentadecanoyl-sn-glycero-3-phosphocholine
1-(1Z-octadecenyl)-2-arachidonoyl-sn-glycero-3-phosphoserine
2,3-bis-O-(geranylgeranyl)-sn-glycero-3-phospho-L-serine
1-linoleoyl-sn-glycero-3-phosphoethanolamine
phosphoethanolamine
Choline Alfoscerate
1-(sn-glycero-3-phospho)-1D-myo-inositol
Glycerol 3-phosphate
Lysophosphatidylinositol
lysophosphatidylserine
Diethanolamine
lysophosphatidylethanolamine (22:6(4Z,7Z,10Z,13Z,16Z,19Z)/0:0)
Glycerophosphoglycerol
O-[{2-[(Diaminomethylene)amino]ethoxy}(hydroxy)phosphoryl]serine
WDC3
WDC1
WDC2
WDsiAATF1
WDsiAATF2
WDsiAATF3

Figure 8

A

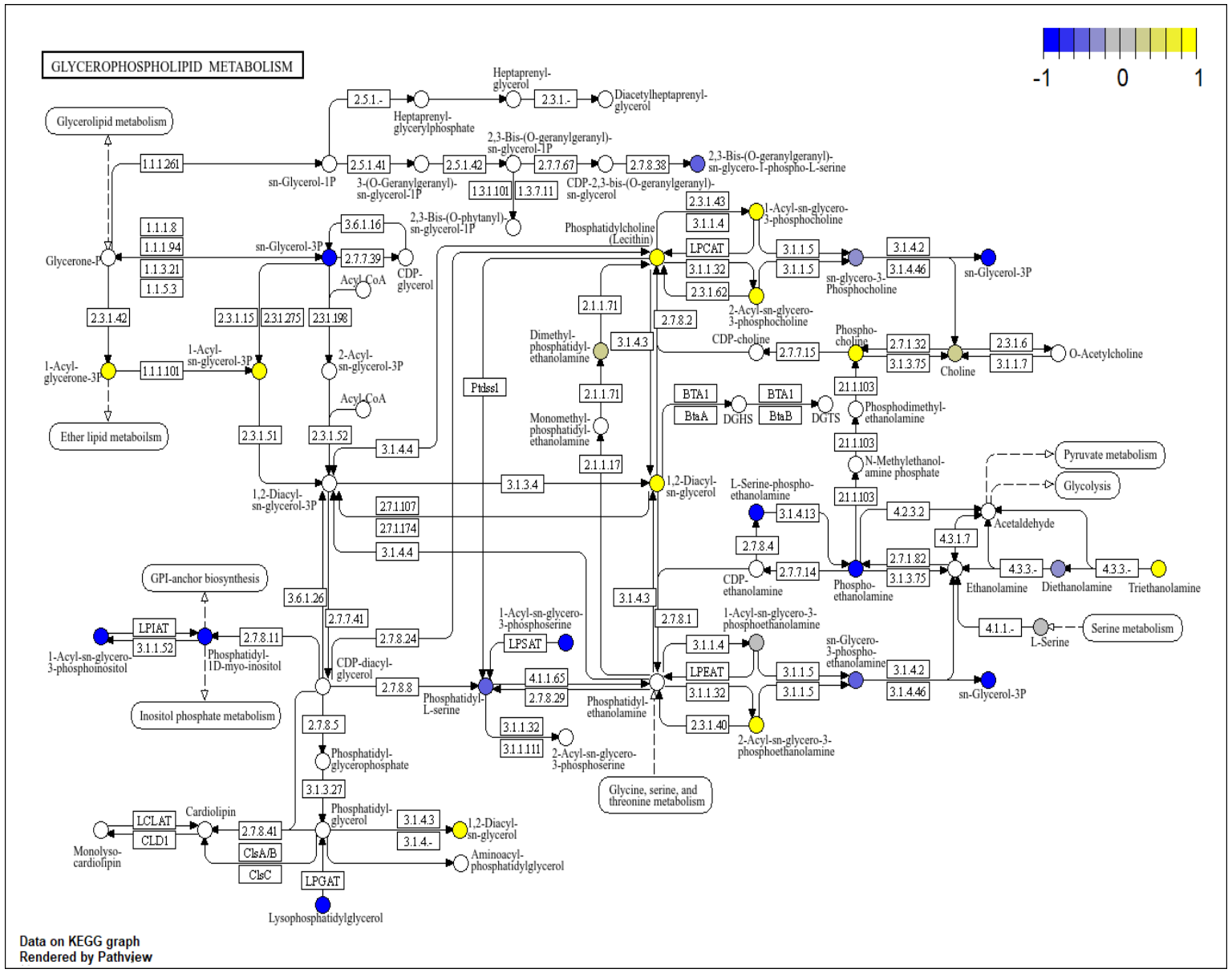
GLYCEROPHOSPHOLIPID METABOLISM
-1
0
1
Glycerolipid metabolism
Glycerone-P
sn-Glycerol-1P
sn-Glycerol-3P
1-Acyl-glycerone-3P
Ether lipid metabolism
1-Acyl-sn-glycerol-3P
2-Acyl-sn-glycerol-3P
1,2-Diacyl-sn-glycerol-3P
1,2-Diacyl-sn-glycerol
Phosphatidylcholine (Lecithin)
1-Acyl-sn-glycero-3-phosphocholine
2-Acyl-sn-glycero-3-phosphocholine
sn-glycero-3-Phosphocholine
Choline
O-Acetylcholine
Phosphocholine
CDP-choline
Dimethylphosphatidylethanolamine
Monomethylphosphatidylethanolamine
Phosphodimethylethanolamine
N-Methylethanolamine phosphate
L-Serine-phosphoethanolamine
CDP-ethanolamine
Phosphoethanolamine
Ethanolamine
Diethanolamine
Triethanolamine
Acetaldehyde
Pyruvate metabolism
Glycolysis
Serine metabolism
L-Serine
1-Acyl-sn-glycero-3-phosphoethanolamine
sn-Glycero-3-phosphoethanolamine
2-Acyl-sn-glycero-3-phosphoethanolamine
GPI-anchor biosynthesis
1-Acyl-sn-glycero-3-phosphoinositol
Phosphatidyl-1ID-myo-inositol
Inositol phosphate metabolism
CDP-diacylglycerol
Phosphatidyl-L-serine
Phosphatidylethanolamine
1-Acyl-sn-glycero-3-phosphoserine
2-Acyl-sn-glycero-3-phosphoserine
Phosphatidylglycerophosphate
Glycine, serine, and threonine metabolism
Cardiolipin
Monolyso-cardiolipin
Phosphatidylglycerol
1,2-Diacyl-sn-glycerol
Aminoacyl-phosphatidylglycerol
Lysophosphatidylglycerol
Data on KEGG graph
Rendered by Pathview

B

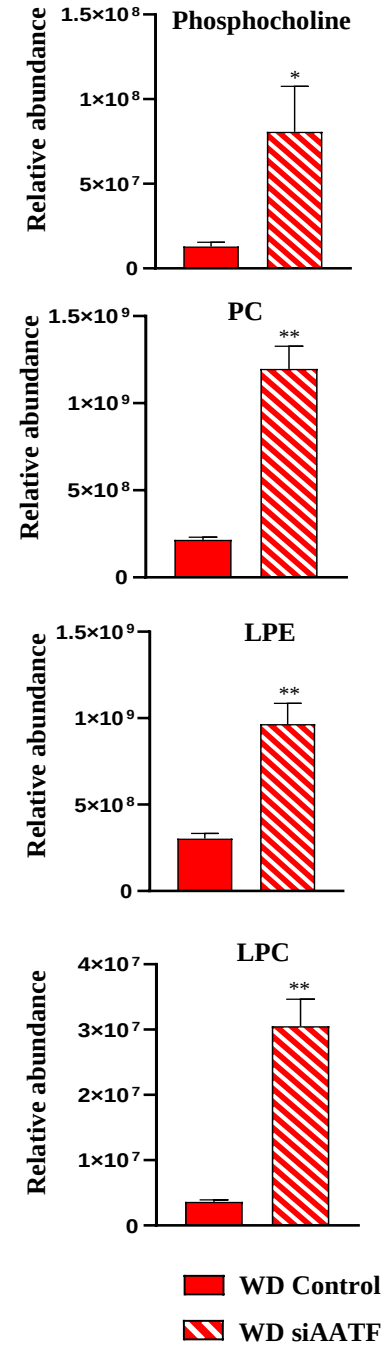
Phosphocholine
PC
LPE
LPC
Relative abundance
1.5×10⁸
1×10⁸
5×10⁷
0
1.5×10⁹
5×10⁸
4×10⁷
3×10⁷
2×10⁷
1×10⁷
*
**
WD Control
WD siAATF

C

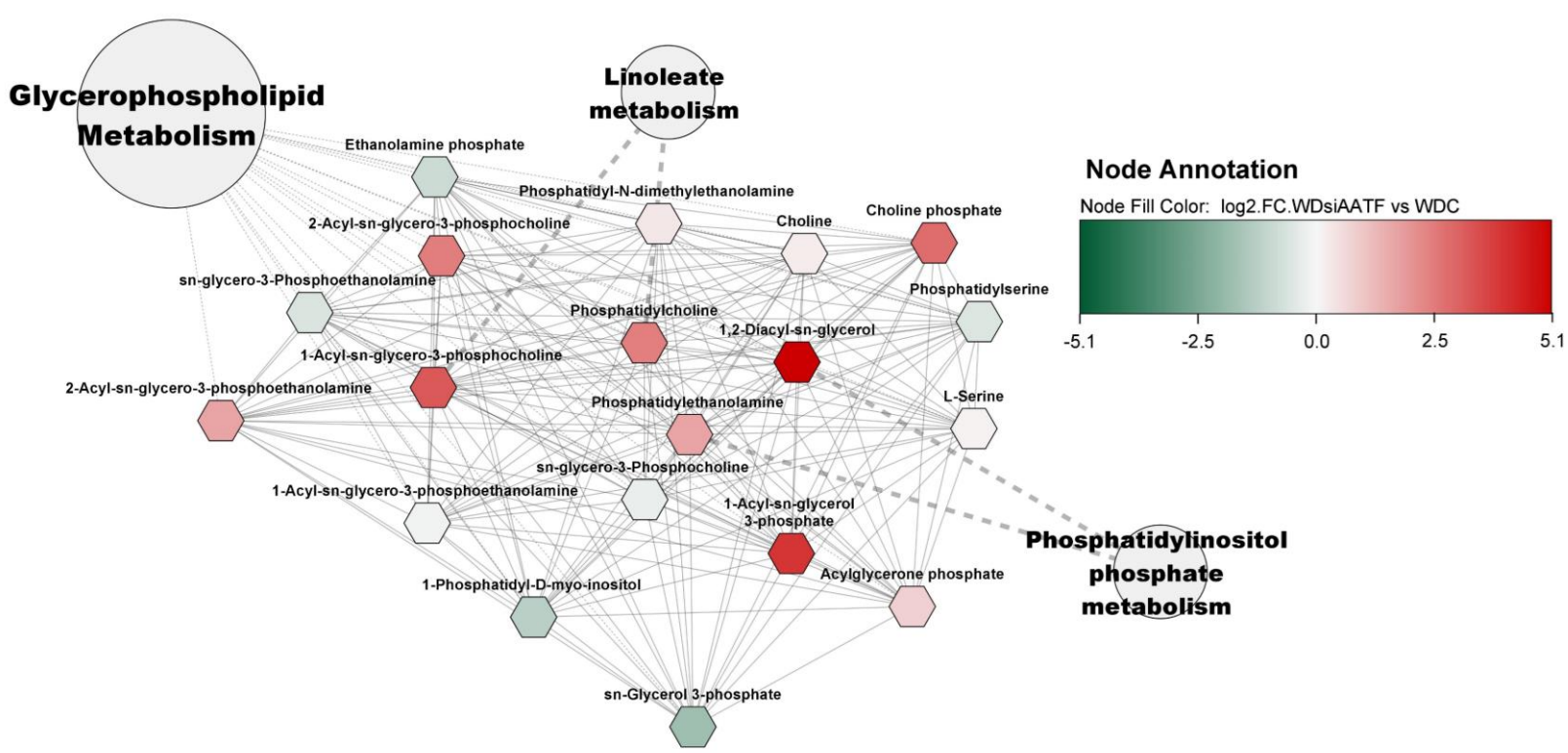
Glycerophospholipid Metabolism
Linoleate metabolism
Phosphatidylinositol phosphate metabolism
Ethanolamine phosphate
Phosphatidyl-N-dimethylethanolamine
Choline
Choline phosphate
2-Acyl-sn-glycero-3-phosphocholine
sn-glycero-3-Phosphoethanolamine
Phosphatidylcholine
Phosphatidylserine
1,2-Diacyl-sn-glycerol
1-Acyl-sn-glycero-3-phosphocholine
2-Acyl-sn-glycero-3-phosphoethanolamine
Phosphatidylethanolamine
L-Serine
sn-glycero-3-Phosphocholine
1-Acyl-sn-glycero-3-phosphoethanolamine
1-Acyl-sn-glycerol 3-phosphate
Acylglycerone phosphate
1-Phosphatidyl-D-myo-inositol
sn-Glycerol 3-phosphate
Node Annotation
Node Fill Color: log2.FC.WDsiAATF vs WDC
-5.1
-2.5
0.0
2.5
5.1

Figure 9

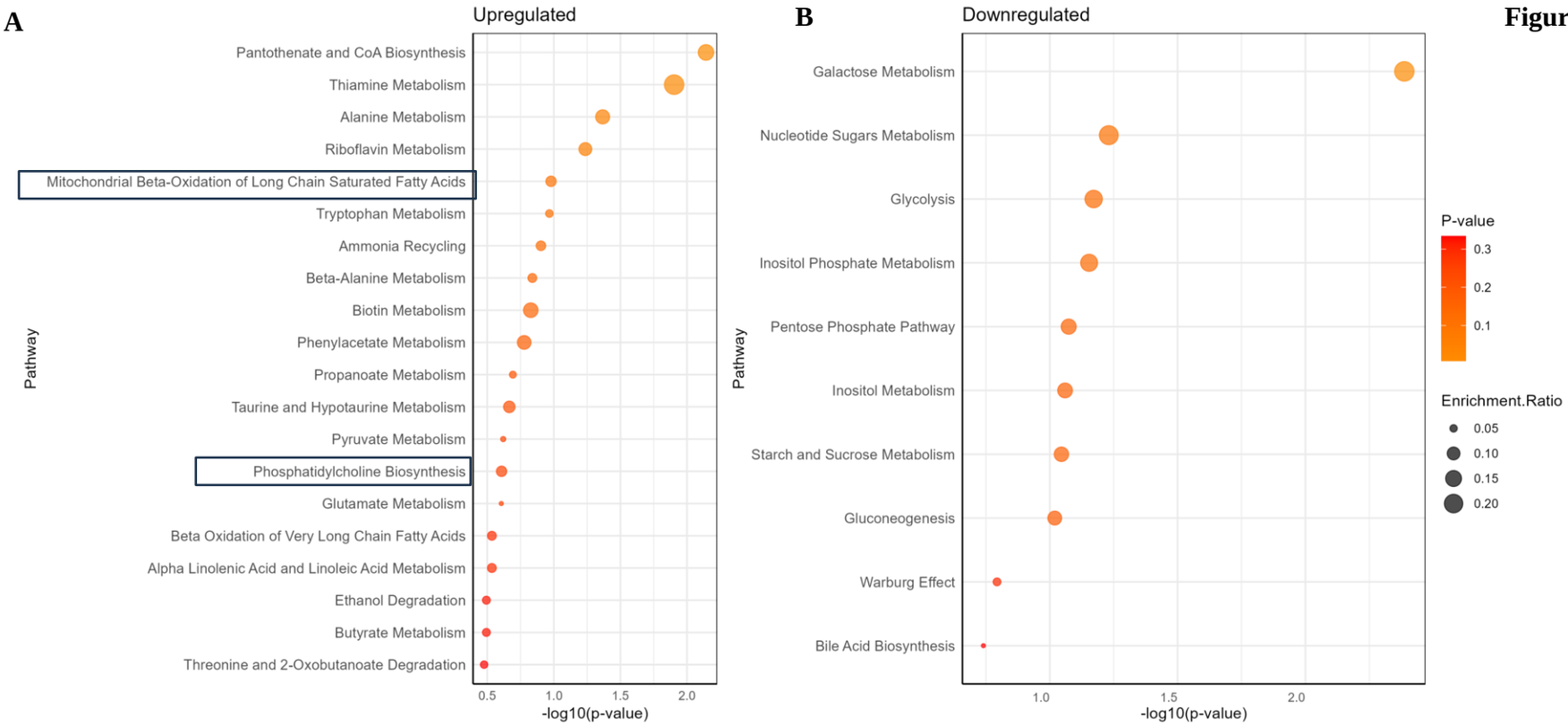
A
Upregulated
Pantothenate and CoA Biosynthesis
Thiamine Metabolism
Alanine Metabolism
Riboflavin Metabolism
Mitochondrial Beta-Oxidation of Long Chain Saturated Fatty Acids
Tryptophan Metabolism
Ammonia Recycling
Beta-Alanine Metabolism
Biotin Metabolism
Phenylacetate Metabolism
Propanoate Metabolism
Taurine and Hypotaurine Metabolism
Pyruvate Metabolism
Phosphatidylcholine Biosynthesis
Glutamate Metabolism
Beta Oxidation of Very Long Chain Fatty Acids
Alpha Linolenic Acid and Linoleic Acid Metabolism
Ethanol Degradation
Butyrate Metabolism
Threonine and 2-Oxobutanoate Degradation
Pathway
0.5
1.0
1.5
2.0
-log10(p-value)
B
Downregulated
Galactose Metabolism
Nucleotide Sugars Metabolism
Glycolysis
Inositol Phosphate Metabolism
Pentose Phosphate Pathway
Inositol Metabolism
Starch and Sucrose Metabolism
Gluconeogenesis
Warburg Effect
Bile Acid Biosynthesis
Pathway
1.0
1.5
2.0
-log10(p-value)
P-value
0.3
0.2
0.1
Enrichment.Ratio
0.05
0.10
0.15
0.20

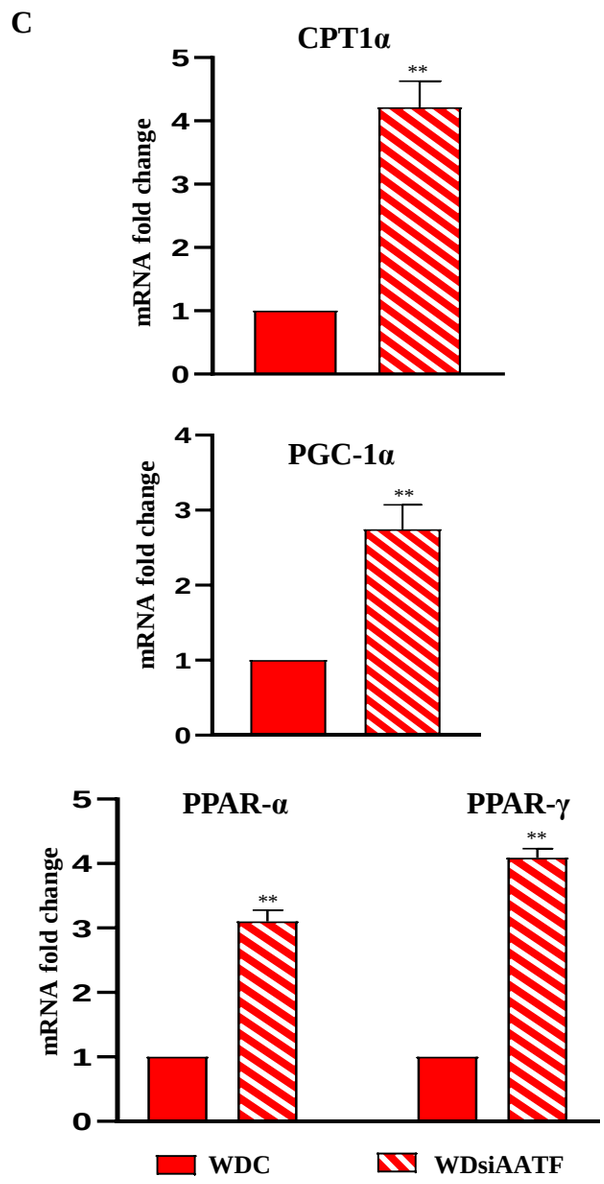
C
CPT1α
mRNA fold change
0
1
2
3
4
5
**
PGC-1α
mRNA fold change
0
1
2
3
4
**
PPAR-α
PPAR-γ
mRNA fold change
0
1
2
3
4
5
**
**
WDC
WDsiAATF

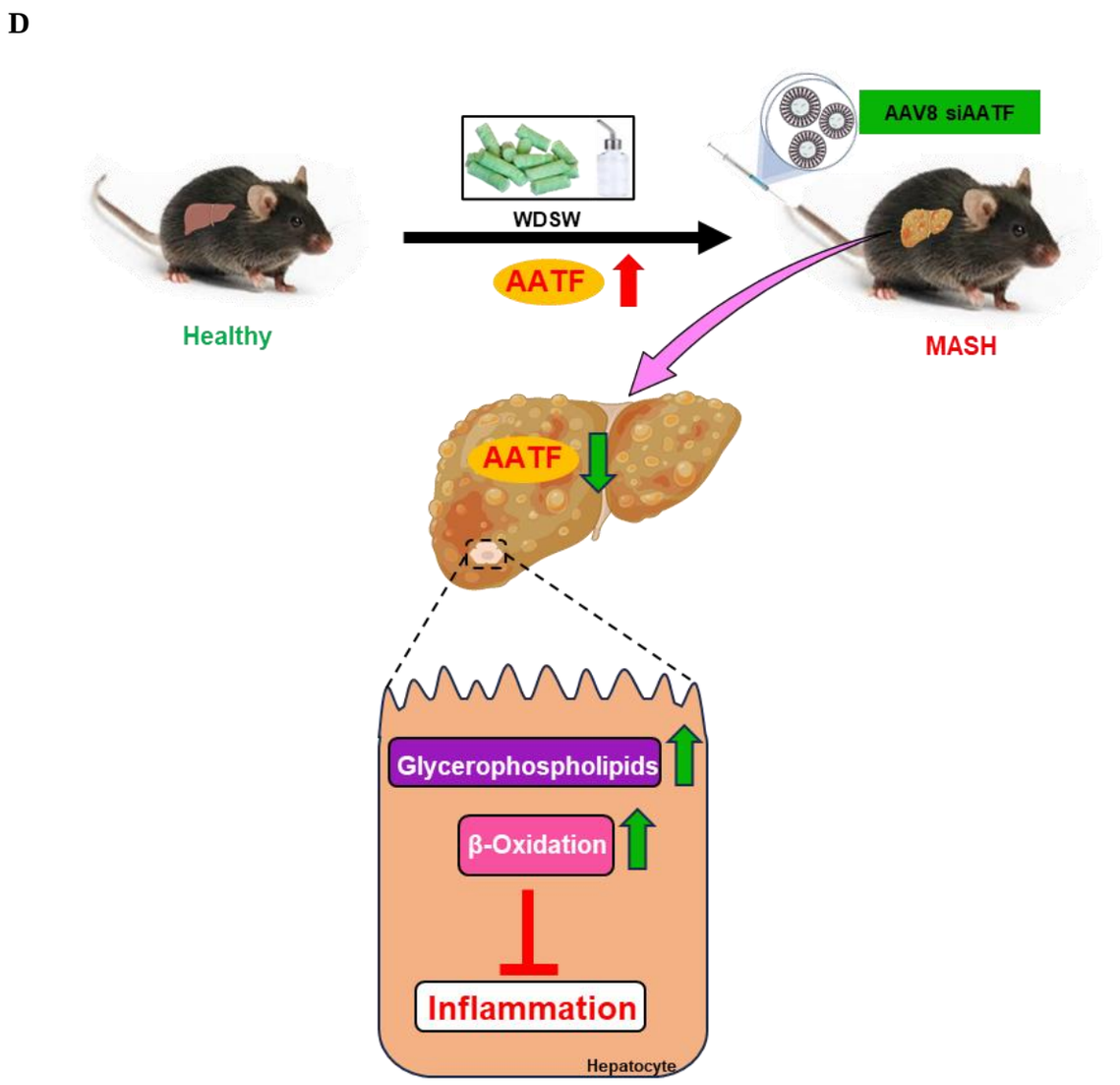
D
Healthy
WDSW
AATF
AAV8 siAATF
MASH
AATF
Glycerophospholipids
β-Oxidation
Inflammation
Hepatocyte